

TimeMosaic: Temporal Heterogeneity Guided Time Series Forecasting via Adaptive Granularity Patch and Segment-wise Decoding

Kuiye Ding¹, Fanda Fan^{1†}, Chunyi Hou², Zheyang Wang³,
Lei Wang¹, Zhengxin Yang¹, Jianfeng Zhan^{1,4}

¹Institute of Computing Technology, Chinese Academy of Sciences

²School of Information Science and Technology, Beijing University of Technology

³Department of Mathematical Sciences, Durham University

⁴University of Chinese Academy of Sciences

{dingkuiye, fanfanda, wanglei_2011, yangzhengxin, zhanjianfeng}@ict.ac.cn,
houchunyi@emails.bjut.edu.cn, zheyang.wang@durham.ac.uk

Abstract

Multivariate time series forecasting is essential in domains such as finance, transportation, climate, and energy. However, existing patch-based methods typically adopt fixed-length segmentation, overlooking the heterogeneity of local temporal dynamics and the decoding heterogeneity of forecasting. Such designs lose details in information-dense regions, introduce redundancy in stable segments, and fail to capture the distinct complexities of short-term and long-term horizons. We propose **TimeMosaic**, a forecasting framework that aims to address temporal heterogeneity. TimeMosaic employs adaptive patch embedding to dynamically adjust granularity according to local information density, balancing motif reuse with structural clarity while preserving temporal continuity. In addition, it introduces segment-wise decoding that treats each prediction horizon as a related subtask and adapts to horizon-specific difficulty and information requirements, rather than applying a single uniform decoder. Extensive evaluations on benchmark datasets demonstrate that TimeMosaic delivers consistent improvements over existing methods, and our model trained on the large-scale corpus with 321 billion observations achieves performance competitive with state-of-the-art TSFMs.

Code — <https://github.com/BenchCouncil/TimeMosaic>

1 Instruction

Multivariate time series forecasting (Yu et al. 2024, 2023; Zheng et al. 2023) plays a critical role in numerous real-world domains (Qiu et al. 2025a,c), such as finance (Zhu et al. 2024a,b), transportation (Shu, Cai, and Xiong 2021), climate (Schneider and Dickinson 1974), healthcare (Morid, Sheng, and Dunbar 2023), and energy management (Liu et al. 2023). These applications require accurate and efficient modeling of intricate temporal relationships among multiple correlated variables. Recently, forecasting methods employing patch-based representations have shown remarkable performance and have become increasingly prevalent (Chen et al. 2024; Jin et al. 2024; Kudrat et al. 2025; Nie et al.

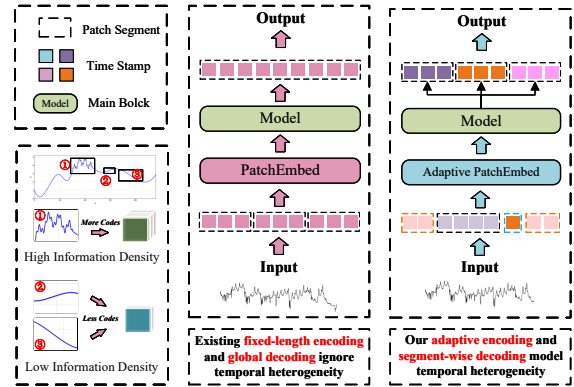


Figure 1: Comparison between existing fixed-patch models and our adaptive patching design, highlighting differences in input representation and prediction structure.

2023). Patch-based approaches excel at capturing localized temporal structures and mitigating noise through segmented encoding. Recently proposed time series models, such as Sundial (Liu et al. 2025), also use patch-based time series segmentation to organize event contexts for benchmarking time series foundation models. Typically, these methods divide input sequences into fixed-length patches, implicitly assuming uniform information density and temporal complexity across the entire sequence.

However, real-world time series often exhibit significant variability in local information density (Huang et al. 2023; Warren Liao 2005). Segments characterized by complex or abrupt changes inherently contain higher information densities, whereas smoother or stationary regions possess relatively lower densities. Current methods employing fixed-size temporal segments disregard this inherent variability, resulting in inadequate modeling of information-rich regions and redundant encoding in smoother ones. Beyond local variability, empirical evidence (Xie et al. 2025) also reveals two key structural properties: *motif reuse*, characterized by Zipf-like frequency distributions, and *structural*

[†]Corresponding author: fanfanda@ict.ac.cn.

clarity, measured by latent-space separability (see Section 2 for definitions and illustrations), which further highlight a structural limitation of fixed-length patching: it cannot simultaneously preserve reusable long-range patterns and maintain well-delimited local boundaries. A similar limitation has been observed in autoregressive image generation, such as DQ-VAE (Huang et al. 2023), where fixed-size region encodings likewise fail to adapt to diverse structural patterns.

These observations indicate that the limitations of fixed-length patching are not incidental but stem from a deeper property of time series data: **heterogeneity**. On the input side, local temporal regions vary greatly in complexity and information density, which we refer to as *encoding heterogeneity*. On the output side, forecasting horizons differ in both difficulty and information requirements, which we refer to as *decoding heterogeneity*. Addressing these two dimensions of heterogeneity is crucial for advancing time series forecasting.

Overall, multivariate time series forecasting faces two fundamental challenges: ① **Encoding heterogeneity**. Fixed-length segmentation fails to adapt to the variability of local temporal complexity, leading to a trade-off between reusing long-term motifs and preserving clear structural boundaries. ② **Decoding heterogeneity**. Forecasting demands differ substantially across horizons: short-term forecasting mainly rely on recent local information, while long-term forecasting require modeling more abstract and uncertain dynamics over broader contexts. Existing methods typically overlook this asymmetry by applying a single decoder to all horizons.

To address these two challenges, we propose **TimeMosaic**, a novel forecasting framework that integrates adaptive patch embedding with segment-wise decoding. On the input side, we design an adaptive granularity patch embedding strategy inspired by dynamic quantization (Huang et al. 2023). Our approach segments input sequences into variable-length patches based on local temporal information density, balancing motif reuse with structural clarity. Unlike prior multi-granularity methods that produce overlapping or re-ordered patches, TimeMosaic ensures that each time step belongs to exactly one patch, thereby preserving strict temporal continuity that is essential for forecasting. As illustrated in Figure 1, fixed-length patching overlooks temporal heterogeneity: it loses details in information-dense regions and introduces redundancy in smooth intervals.

On the output side, we introduce a segment-wise prediction framework based on multi-task prompt tuning (Liu et al. 2021; Crawshaw 2020a). By treating different horizons as distinct yet related subtasks, our method equips the model with segment-aware prompt embeddings that capture horizon-specific difficulty and information requirements without modifying the backbone parameters. This design enables specialization across prediction segments, effectively leveraging the rich and heterogeneous information captured by adaptive patches. As illustrated in Figure 1, TimeMosaic adopting segment-wise forecasting that treats each horizon as a dedicated subtask.

We summarized our main contributions as follows:

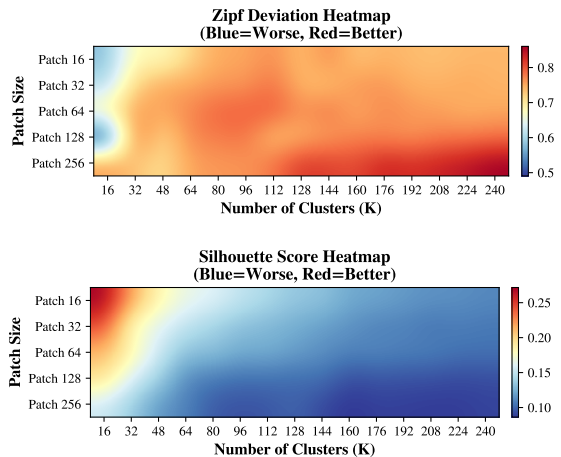


Figure 2: Zipf deviation and Silhouette score. These results are obtained by extracting patches of different lengths from a large-scale collection of time series forecasting datasets (see Appendix A), followed by K-Means clustering under various cluster settings.

- We propose **TimeMosaic**, a novel forecasting framework that explicitly addresses both encoding heterogeneity and decoding heterogeneity in multivariate time series.
- We design an Adaptive Patch Embedding module that dynamically allocates region-specific patch sizes according to local information density, effectively balancing motif reuse with structural clarity.
- We introduce a segment-wise prompt tuning strategy that models horizon-specific difficulty and information requirements by treating each prediction segment as a distinct subtask within a unified multi-task framework.
- We conduct extensive experiments across 9 real-world datasets, showing that TimeMosaic achieves state-of-the-art performance in long-term forecasting.

2 Related Work

Patch-based Time Series Forecasting. Recent advances in time series forecasting have been driven by patch-based representations. PatchTST (Nie et al. 2023) first introduced temporal patches into Transformer-based models, followed by Patchwise (Kudrat et al. 2025), which utilized local statistics, and TimeFilter (Hu et al. 2025), which applied fine-grained filtration. Time-LLM (Jin et al. 2024) further demonstrated the utility of patches in LLM-based forecasting. However, all these models adopt fixed-length patching, assuming uniform temporal complexity and lacking flexibility to adapt to local variations.

To overcome this limitation, multi-granularity patching has been explored. PatchMLP (Tang and Zhang 2025) introduced multiple segment lengths to enrich temporal features, while PathFormer (Chen et al. 2024) and DualSG (Ding et al. 2025) selected patch sizes based on importance scores or maps. Although effective, these methods may break temporal consistency due to overlapping or misordered patches. For instance, coarse patches can appear earlier than fine ones

in the sequence, distorting input chronology and undermining forecasting coherence, see Appendix Figure 7.

In contrast, our method introduces adaptive patch embedding with strict temporal alignment, dynamically adjusting patch sizes based on local information density while preserving the original time order.

Zipf Conformity and Clustering Clarity. Recent research (Xie et al. 2025) shows that temporal patches in time series follow a Zipf-like frequency distribution (Axtell 2001), exhibit clear clustering properties (measured by Silhouette scores (Rousseeuw 1987)), and display strong sequential dependencies. Zipf conformity reveals the emergence of reusable temporal motifs, enabling compact representation and pattern reuse, while structural clarity reflects how distinctly different temporal patterns can be separated in latent space, facilitating stable representation learning and reliable generalization.

Building on these findings, we identify a key trade-off: fixed-length segmentation cannot optimize Zipf conformity and clustering clarity at the same time. Larger patches capture longer recurring patterns and thus improve Zipf conformity, but they blur behavioral boundaries. In contrast, smaller patches sharpen clustering clarity, yet they fragment long-term patterns and reduce reuse, as shown in Figure 2.

Autoregressive Forecasting Paradigm. Autoregressive (AR) models (Lin et al. 2023; Khaldi et al. 2023; Stankeviciute, M Alaa, and Van der Schaar 2021) such as RNNs and LSTMs (Kong et al. 2025; Yadav and Thakkar 2024) have long dominated time series forecasting. Even recent foundation models (Shi et al. 2025; Liu et al. 2024b; Ansari et al. 2024) largely follow the AR formulation. However, these methods suffer from exposure bias (Ranzato et al. 2016) and equal treatment of short- and long-term predictions, despite their differing complexity and uncertainty.

Our approach departs from this paradigm by adopting a segment-wise multi-task formulation. This design avoids recursive error accumulation and allows segment-specific specialization, addressing both exposure bias and forecasting asymmetry.

Multi-task Learning and Prompt-based Adaptation. Multi-task learning (MTL) (Ruder 2017; Crawshaw 2020b) enhances generalization by sharing knowledge across tasks. In the context of large language models, it has been applied to summarization (Laban et al. 2023), QA (Zhuang et al. 2023), and sentiment analysis (Zhang et al. 2024; Cao et al. 2024), often in combination with parameter-efficient methods like LoRA (Xia et al. 2024) and prompt tuning (Lester, Al-Rfou, and Constant 2021).

We follow this trend by introducing prompt-based MTL into time series forecasting. Compared to basis-reconstruction methods such as TimeBase (Huang et al. 2025), which rely on strong periodicity assumptions and static segment structures, our model learns dynamic, segment-aware prompts for flexible and efficient temporal adaptation. This enables better modeling of local heterogeneity without assuming low-rank structure or modifying the shared encoder.

3 Preliminaries and Definition

Preliminaries. In multivariate time series forecasting, we are given a historical sequence $\mathbf{X} \in \mathbb{R}^{C \times L}$, where C is the number of channels and L is the number of past timesteps. The goal is to predict the future H steps, denoted as $\mathbf{Y} \in \mathbb{R}^{C \times H}$. A forecasting model learns a mapping $f: \mathbb{R}^{C \times L} \rightarrow \mathbb{R}^{C \times H}$ from past observations to future values.

Temporal heterogeneity. Temporal heterogeneity refers to the non-uniform characteristics of time series across different temporal regions, encompassing both input-side variability and output-side forecasting challenges. On the input side, real-world sequences exhibit varying local complexity—volatile regions contain rapid fluctuations requiring fine-grained modeling, while stable segments allow for coarser abstraction. On the output side, prediction targets across different horizons pose asymmetric difficulties: short-term predictions often rely on recent patterns, whereas long-term predictions involve more abstract, uncertain dynamics. Ignoring such heterogeneity leads to suboptimal representations and a mismatch between model capacity and forecasting needs.

4 Proposed Method

4.1 Rethinking Temporal Heterogeneity in Time Series Encoding and Decoding

Real-world time series exhibit varying local complexity and asymmetric forecasting difficulty. Existing patch-based models typically adopt fixed-length segmentation, assuming uniform temporal dynamics. However, volatile regions demand fine-grained modeling, while smooth segments can be coarsely encoded; using a single patch size thus leads to either detail loss or redundant computation. This motivates a rethinking of both encoding and decoding strategies.

Forecasting over long horizons further introduces diverse semantic demands: early segments rely on recent trends, whereas distant predictions involve more abstract and uncertain dynamics. Yet most models decode all horizons with a shared head, ignoring this temporal asymmetry.

To address these challenges, we propose (1) an adaptive patch embedding module that learns region-specific granularity from local information density, and (2) a segment-wise prompt tuning framework that treats each forecast segment as a subtask. This design enables input-aware encoding and horizon-specific specialization, improving performance and robustness while maintaining parameter efficiency.

4.2 Method Overview

We propose a forecasting framework that combines adaptive patch embedding and segment-wise prompt tuning. The model first partitions the input into fixed-length regions, then selects a patch size per region from a candidate set. This yields variable-length patch sequences aligned to a uniform format via replication, enabling Transformer-compatible processing while preserving temporal coherence.

To forecast multi-step targets, we treat each future segment as a distinct subtask and assign it a learnable prompt.

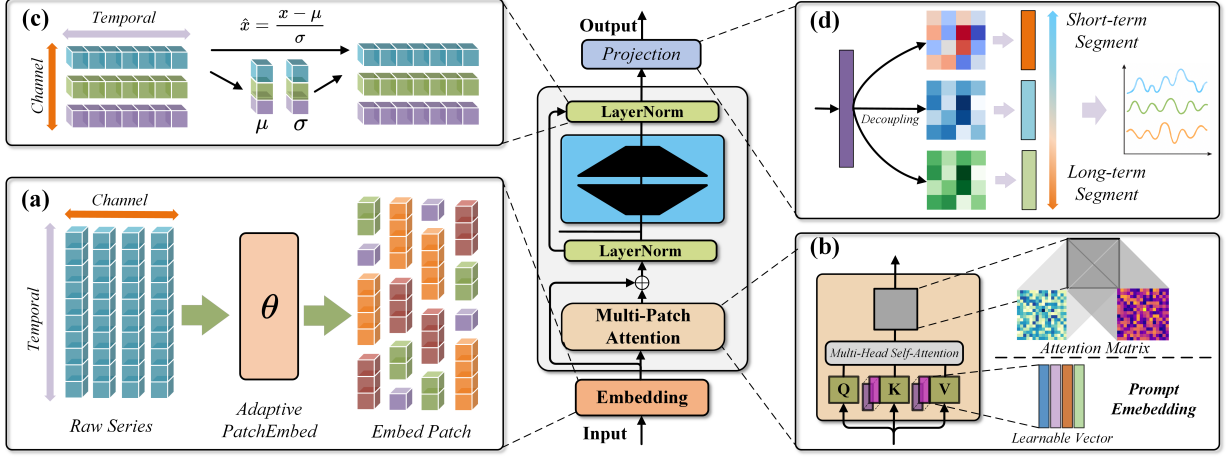


Figure 3: Overall architecture of TimeMosaic, which shares the same modular arrangement with the encoder of Transformer. (a) The input multivariate time series is first processed by the Adaptive Patch Embedding module, which segments the sequence into patches of varying granularity based on learnable region-wise decisions. (b) A set of learnable prompt tokens are injected into the input sequence and interact with patch embeddings via multi-head attention to guide segment-wise forecasting. The attention maps in this panel visualize the interactions among adaptive patches as well as between patches and prompts. (c) Input sequence are normalized at the Channel level, same as iTransformer (Liu et al. 2024a). (d) The model performs segment-wise forecasting, from the short-term to the long-term.

These prompts inject segment-specific biases into a shared encoder, allowing the model to specialize without altering backbone parameters. Additionally, we support both channel-independent and channel-dependent processing to flexibly handle inter-variable correlations. The entire framework is trained end-to-end with a loss that balances forecasting accuracy and patch usage diversity.

4.3 Adaptive Patch Embedding

To effectively model temporal heterogeneity in time series, we introduce an Adaptive Patch Embedding (APE) module that adjusts patch granularity based on local dynamics.

Patch Granularity Search Space. We refer to *regions* as local partitions of the input used for adaptive patching, and *segments* as forecast sub-horizons used in multi-task prediction. This distinction allows us to separately model spatial encoding and temporal decoding. Given an input time series $x \in \mathbb{R}^{B \times C \times L}$, we divide the sequence into $R = L/f_{\max}$ non-overlapping regions, where f_{\max} is the maximum patch length in the candidate set:

$$\mathcal{F} = \{f_1, f_2, \dots, f_K\}, \quad f_1 < f_2 < \dots < f_K. \quad (1)$$

Each candidate patch size f_k represents a different temporal granularity. For each region, our goal is to select the most suitable f_k to match its local information density.

Region-wise Granularity Classification. To predict the optimal patch size for each region, we employ a lightweight classifier \mathcal{G}_θ :

$$g_r = \mathcal{G}_\theta(x_r) \in \mathbb{R}^K, \quad \theta_r = \arg \max_k g_{r,k}, \quad (2)$$

where g_r is the predicted logits over candidate patch sizes for region x_r , and θ_r is the index of the selected patch size.

The classifier is shared across all regions and channels, and is implemented as a two-layer MLP. To ensure end-to-end differentiability, we apply the Gumbel-Softmax (Jang, Gu, and Poole 2017) during training.

Patch Alignment and Embedding. After determining the patch size f_{θ_r} for region x_r , we unfold it into patches of size f_{θ_r} :

$$z_r = \text{Linear}_{f_{\theta_r}}(\text{Unfold}(x_r; f_{\theta_r})) \in \mathbb{R}^{N_r \times d}, \quad (3)$$

where z_r is the embedded patch sequence, $N_r = f_{\max}/f_{\theta_r}$ is the number of patches in region r , and d is the embedding dimension. Each patch is projected to a shared latent dimension d using a dedicated linear layer.

To maintain a uniform input shape across regions, we up-sample all patch sequences to a fixed length $N = f_{\max}/f_{\min}$ using replication:

$$\tilde{z}_r = \text{RepeatPad}(z_r; N). \quad (4)$$

where \tilde{z}_r is the length-aligned patch sequence for region r , padded to $N = f_{\max}/f_{\min}$ using replication. RepeatPad preserves temporal alignment and avoids introducing artificial content. In practice, we find it more stable than interpolation or learned resampling under varying patch configurations.

All region patch embeddings $\{\tilde{z}_1, \dots, \tilde{z}_R\}$ are concatenated and enriched with positional encodings to form the final input:

$$Z = \text{PE}(\text{Concat}(\tilde{z}_1, \dots, \tilde{z}_R)) \in \mathbb{R}^{B \cdot C \times N \cdot R \times d}. \quad (5)$$

where Z is the final encoder input sequence after adding positional encodings, $\text{PE}(\cdot)$ denotes the positional encoding function, and R is the number of input regions. We explore

several alternative designs for positional encoding, including fixed, learnable, and hybrid schemes, which are analyzed in Section 5.

Regularization via Budget Loss Without constraints, the classifier may degenerate to always selecting the finest patch size. To avoid this, we introduce a *budget loss* to match the empirical distribution of selected granularities to a predefined target:

$$\mathcal{L}_{\text{budget}} = \sum_{k=1}^{K-1} (r_k - \hat{r}_k)^2, \quad (6)$$

where r_k is the desired usage ratio of patch size f_k , and \hat{r}_k is the actual usage in the current batch. The last ratio is defined by normalization:

$$r_K = 1 - \sum_{k=1}^{K-1} r_k, \quad \hat{r}_K = 1 - \sum_{k=1}^{K-1} \hat{r}_k. \quad (7)$$

Training Objective. We jointly optimize the forecasting loss and the budget regularization. The total training loss is defined as:

$$\mathcal{L}_{\text{total}} = \mathcal{L}_{\text{forecast}} + \lambda \mathcal{L}_{\text{budget}}, \quad (8)$$

where $\mathcal{L}_{\text{forecast}}$ is the standard mean squared error (MSE) between the prediction \hat{y} and ground truth y :

$$\mathcal{L}_{\text{forecast}} = \frac{1}{B} \sum_{i=1}^B \|\hat{y}^{(i)} - y^{(i)}\|_2^2. \quad (9)$$

λ is a hyperparameter balancing the two terms.

4.4 Prompt Tuning for Segment-wise Forecasting

We formulate multi-interval time series forecasting as a segment-wise multitask learning problem, where each forecast segment corresponds to an individual prediction subtask. To achieve parameter-efficient segment adaptation, we draw inspiration from Prompt Tuning (Lester, Al-Rfou, and Constant 2021; Liu et al. 2021) and extend it to the temporal domain. Specifically, we design learnable segment-aware prompts to inject segment-specific inductive biases into a shared encoder, allowing the model to specialize its attention behavior for each segment without modifying backbone parameters.

Following standard practices in prompt tuning, these prompts are inserted only into the key and value paths of the attention mechanism, while the query vectors are derived exclusively from the input data. This asymmetric design ensures that the original data tokens retain their semantic role as information seekers, while prompts act as soft guidance to steer the attention focus in a segment-aware manner. Compared with adapter-based or decoder-tuning approaches, prompt tuning achieves similar segment-level specialization with fewer trainable parameters and better modularity, as prompts can be flexibly added or removed without altering the shared encoder.

For a given segment $k \in \{1, \dots, K\}$, we associate a prompt embedding $\phi_k \in \mathbb{R}^{l \times d}$ and prepend it to the input representation $\mathbf{X} \in \mathbb{R}^{n \times d}$:

$$\tilde{\mathbf{X}}_k = \text{Concat}(\phi_k, \mathbf{X}). \quad (10)$$

To preserve a clear functional separation between prompts and data tokens, we apply a prompt-masked attention mechanism. In the self-attention computation, query vectors are derived exclusively from data tokens, while key and value vectors include both data and prompts:

$$\mathbf{Q}_k = \mathbf{X}W^Q, \quad \mathbf{K}_k = \tilde{\mathbf{X}}_k W^K, \quad \mathbf{V}_k = \tilde{\mathbf{X}}_k W^V. \quad (11)$$

This allows the segment-aware prompt to modulate attention flow and inject task-relevant semantics, while being excluded from explicit decoding.

After encoding, each segment is decoded by a segment-specific head $f_k(\cdot; \theta_k)$, yielding the prediction $\hat{\mathbf{Y}}^{(k)} \in \mathbb{R}^{m_k \times C}$:

$$\hat{\mathbf{Y}}^{(k)} = f_k(\mathbf{H}_k; \theta_k), \quad (12)$$

where \mathbf{H}_k is the shared encoder output.

This segment-wise prompt tuning framework enables flexible modeling of segment-specific dynamics, improves parameter efficiency, and avoids interference across subtasks. All encoder parameters remain frozen during training, and only prompts $\{\phi_k\}$ and decoding heads $\{\theta_k\}$ are updated.

5 Experiments

We thoroughly evaluate the proposed TimeMosaic on various time series forecasting applications, validate the generality of the proposed framework and further delve into the effectiveness of adaptive patch embedding and Segment-wise Forecasting in other models.

Datasets. We conduct extensive experiments on 17 real-world multivariate time series datasets, which are divided into long-term and short-term forecasting tasks. For long-term forecasting, we use ETTh1, ETTh2, ETTm1, ETTm2 (Zhou et al. 2021), Weather, Traffic, Electricity, ExchangeRate (Wu et al. 2023), Solar-Energy (Lai et al. 2018), and Wind (Location1–4) (Xie et al. 2025). For short-term forecasting, we adopt four benchmark traffic datasets: PEMS03, PEMS04, PEMS07, and PEMS08 (Wang et al. 2024, 2025b).

Baselines. We choose the last state-of-the-art LTSF models, including TimeFilter (Hu et al. 2025), SimpleTM (Chen et al. 2025), PatchMLP (Tang and Zhang 2025), xPatch (Stitsyuk and Choi 2025), DUET (Qiu et al. 2025b), PathFormer (Chen et al. 2024), iTransformer (Liu et al. 2024a), TimeMixer (Wang et al. 2024), PatchTST (Nie et al. 2023), FreTS (Yi et al. 2023), DLinear (Zeng et al. 2023), LightTS (Zhang et al. 2022) as baselines for our experiments. We compared the ability of zero-shot with the GPT4TS (Zhou et al. 2023) and LLMTime (Nate Gruver and Wilson 2023). And we compare against pre-trained foundation time series models, including TimeMoE (Shi et al. 2025), MOIRAI (Woo et al. 2024), Chronos (Ansari et al. 2024), TimesFM (Das et al. 2024), and Moment (Goswami et al. 2024), using the parameter settings as specified in their respective publications.

Evaluation Metrics. Following previous works, we use Mean Squared Error (MSE) and Mean Absolute Error (MAE) metrics to assess the performance.

Models	TimeMosaic (Ours)		SimpleTM (2025)		TimeFilter (2025)		xPatch (2025)		PatchMLP (2025)		DUET (2025)		PathFormer (2024)		iTransformer (2024)		TimeMixer (2024)		PatchTST (2023)		DLinear (2023)	
	MSE	MAE	MSE	MAE	MSE	MAE	MSE	MAE	MSE	MAE	MSE	MAE	MSE	MAE	MSE	MAE	MSE	MAE	MSE	MAE	MSE	MAE
ETTh1	0.381	0.381	0.391	0.403	0.395	0.407	0.391	0.402	0.401	0.407	0.416	0.407	0.392	<u>0.385</u>	0.409	0.411	<u>0.381</u>	0.396	0.387	0.398	0.407	0.409
ETTh2	<u>0.273</u>	0.314	0.283	0.325	0.282	0.329	0.283	0.327	0.287	0.331	0.286	0.328	0.269	<u>0.314</u>	0.293	0.334	0.279	0.325	0.279	0.323	0.350	0.400
ETTm1	0.425	0.424	0.442	0.436	0.463	0.447	0.446	0.439	0.455	0.445	0.447	0.440	0.454	<u>0.428</u>	0.450	0.442	0.445	0.439	<u>0.432</u>	0.431	0.462	0.459
ETTm2	0.363	0.388	0.424	0.413	0.389	0.422	0.409	0.405	0.402	0.416	0.379	0.400	<u>0.372</u>	<u>0.397</u>	0.386	0.407	0.381	0.404	0.376	0.402	0.556	0.516
Weather	<u>0.251</u>	<u>0.267</u>	0.258	0.282	0.242	0.273	0.264	0.284	0.254	0.289	0.269	0.304	0.242	0.266	0.346	0.276	0.309	0.360	0.264	0.283	0.265	0.317
Traffic	<u>0.458</u>	0.283	0.545	0.347	0.461	0.309	0.520	0.335	0.495	0.337	0.628	0.392	0.581	0.343	0.453	0.303	0.499	<u>0.291</u>	0.486	0.314	0.627	0.387
Electricity	0.187	<u>0.279</u>	0.248	0.284	0.170	0.266	0.209	0.292	0.224	0.289	0.216	0.311	0.214	0.293	0.225	0.310	<u>0.185</u>	0.294	0.205	0.292	0.215	0.305
Exchange	0.348	<u>0.403</u>	0.356	0.411	0.366	0.411	0.372	0.410	0.374	0.412	0.356	0.400	0.375	0.411	0.366	0.414	0.385	0.423	0.359	0.401	<u>0.354</u>	0.420
Solar	0.240	<u>0.270</u>	0.315	0.333	<u>0.248</u>	<u>0.270</u>	<u>0.248</u>	0.276	0.255	0.280	0.349	0.350	0.255	0.258	0.378	0.350	0.292	0.281	0.326	0.397	0.256	0.304

Table 1: Averaged forecasting results under unified experimental settings. For **long-term** forecasting tasks, we use a fixed lookback window of $L = 96$. Long-term forecasting results are averaged over four prediction lengths: $T = \{96, 192, 336, 720\}$. The best model is in **boldface**, and the second best is underlined. See Table 20 in Appendix G for complete results.

Channel Modeling Strategy. Although our core design centers on segment-wise forecasting with adaptive patch granularity, handling multivariate inputs remains essential. To ensure compatibility, we incorporate a modular *channel modeling component*, which supports both Channel-Independent (CI) (Nie et al. 2023) and Channel-Dependent (CD) (Hu et al. 2025) schemes. Specifically, we provide multiple instantiations ranging from simple per-variable modeling to prompt-augmented or calendar-aware variants. These options are fully pluggable and do not interfere with the main forecasting pipeline. By default, we adopt the Channel dependent strategy. A comprehensive description and comparison of all variants are provided in Appendix D.

Implementation Details. All the experiments are implemented in PyTorch (Paszke et al. 2019), and conducted on eight A800 GPU. Even in recent studies, it is common to set $drop_last = True$ during data preprocessing (Chen et al. 2025; Wang et al. 2025a), and this issue has been explicitly discussed in the TFB (Qiu et al. 2024), highlighting its potential impact on evaluation fairness. Following the time series forecasting benchmark TFB’s settings (Qiu et al. 2024), we do not use the “drop last” trick during the testing phase to ensure a fair comparison. Our benchmark comprehensively includes 20+ state-of-the-art forecasting models across 17 real-world datasets, ensuring a fair comparison by unifying implementation settings and avoiding over-tuning parameter. And some approaches (Hu et al. 2025) discard the use of *EarlyStopping*, which in our view disregards the essential role of the validation set. Therefore, when integrating with other methods, we consistently retain this setting to ensure fair and reliable evaluation.

Model Variant	MSE	MAE
Baseline	0.277	0.326
+ Adaptive Patch Embedding (APE)	0.258	0.302
+ APE and Segment-wise Prompt Tuning	0.254	0.301

Table 2: Ablation study of each component on five datasets. See datils in Appendix Table 14.

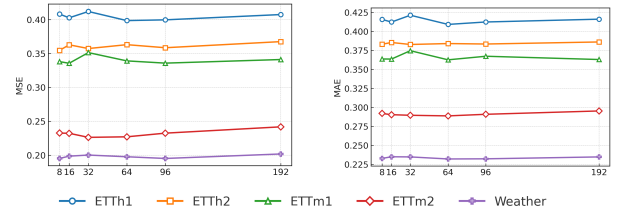


Figure 4: Segments of different sizes on five datasets with a prediction length of 192. Left: MSE. Right: MAE.

Granularity	MSE	MAE
$[8, 16]$	0.231	0.288
$[8, 32]$	0.228	0.286
$[8, 16, 32]$	0.232	0.290
$[8, 16, 64]$	0.230	0.289
$[8, 32, 64]$	0.235	0.289
$[4, 8, 16, 32]$	0.232	0.290
$[8, 16, 32, 64]$	0.228	0.286

Table 3: Impact of patch granularity on six datasets, see details in Appendix Table 13.

Unified Experimental Settings. To ensure fair comparison, we conduct two types of experiments. For long-term forecasting, we follow the unified evaluation protocol proposed by TimesNet (Wu et al. 2023), using a lookback length $L = 96$ and prediction lengths $T = 96, 192, 336, 720$ across all long-term datasets. For short-term forecasting, we adopt a fixed prediction length $T = 12$, which is commonly used in traffic prediction tasks. The lookback length is also set to $L = 96$. The averaged results under this unified setting are reported in Table 1. Table 1 presents results across all models using best configurations obtained via hyperparameter tuning, including the number of layers, attention heads, hidden dimension (d_{model}), and feedforward dimension (d_{ff}), with a lookback window of 96. In contrast, Table 5 reports results with an identical parameter setting shared by all models, using a longer lookback window of 320.

Methods	TimeMosaic		TimeMoE _l		TimeMoE _b		MOIRAI _l		MOIRAI _b		Chronos _b		Chronos _s		TimesFM		Moment		
Metric	MSE	MAE	MSE	MAE	MSE	MAE	MSE	MAE	MSE	MAE	MSE	MAE	MSE	MAE	MSE	MAE	MSE	MAE	
ETTh1	96	0.367	0.395	0.350	0.382	<u>0.357</u>	<u>0.381</u>	0.381	0.388	0.376	0.392	0.384	0.379	0.394	<u>0.381</u>	0.414	0.404	0.688	0.557
	192	0.395	<u>0.412</u>	<u>0.388</u>	<u>0.412</u>	0.384	0.404	0.434	0.415	0.412	0.413	0.441	<u>0.412</u>	0.455	0.414	0.465	0.434	0.688	0.560
	336	0.410	0.423	<u>0.411</u>	0.430	<u>0.411</u>	0.434	0.495	0.445	0.433	<u>0.428</u>	0.475	0.430	0.499	0.444	0.503	0.456	0.675	0.563
	720	0.422	0.443	<u>0.427</u>	0.455	0.449	0.477	0.611	0.510	0.447	<u>0.444</u>	0.472	0.446	0.520	0.476	0.511	0.481	0.683	0.585
	Avg	<u>0.399</u>	<u>0.418</u>	0.394	0.419	0.400	0.424	0.480	0.439	0.417	0.419	0.443	0.416	0.467	0.428	0.473	0.443	0.683	0.566
ETTh2	96	0.190	0.276	0.197	0.286	0.201	0.291	0.211	<u>0.274</u>	0.205	<u>0.273</u>	0.177	0.244	<u>0.180</u>	0.251	0.202	0.270	0.260	0.335
	192	0.249	0.313	0.250	0.322	0.258	0.334	0.281	0.318	0.275	0.316	<u>0.251</u>	0.293	<u>0.251</u>	<u>0.298</u>	0.289	0.321	0.289	0.350
	336	0.305	0.347	0.337	0.375	0.324	0.373	0.341	0.355	0.329	0.350	0.305	0.327	<u>0.315</u>	<u>0.338</u>	0.360	0.366	0.324	0.369
	720	<u>0.396</u>	0.407	0.480	0.461	0.488	0.464	0.428	<u>0.428</u>	0.437	<u>0.411</u>	0.419	0.394	0.421	0.403	0.462	0.430	0.394	0.409
	Avg	0.285	0.336	0.316	0.361	0.317	0.365	<u>0.315</u>	0.343	0.311	<u>0.337</u>	<u>0.288</u>	0.314	0.291	0.330	0.328	0.346	0.316	0.365

Table 4: Zero-shot forecasting results on two datasets. TimeMosaic is trained with an input length of 512 and an output horizon of 720. The symbols *s*, *b*, and *l* represent the small, base, and large versions, respectively. See details in Appendix Table 24

Models	TimeMosaic (Ours)		SimpleTM (2025)		TimeFilter (2025)		xPatch (2025)		PatchMLP (2025)		DUET (2025)		iTransformer (2024)		TimeMixer (2024)		PatchTST (2023)		DLinear (2023)		FreTS (2023)	
Metric	MSE	MAE	MSE	MAE	MSE	MAE	MSE	MAE	MSE	MAE	MSE	MAE	MSE	MAE	MSE	MAE	MSE	MAE	MSE	MAE	MSE	MAE
ETTh1	0.360	0.377	0.350	<u>0.379</u>	0.399	0.408	<u>0.354</u>	0.386	0.374	0.396	0.360	0.380	0.386	0.406	0.356	0.385	0.372	0.399	0.357	0.380	0.369	0.391
ETTh2	0.256	0.310	0.263	0.318	0.278	0.330	0.262	0.322	0.269	0.324	<u>0.257</u>	<u>0.314</u>	0.293	0.338	0.265	0.323	0.278	0.332	0.282	0.348	0.284	0.339
ETTh1	0.412	0.423	0.428	0.438	0.511	0.482	0.446	0.445	0.462	0.460	<u>0.414</u>	<u>0.429</u>	0.487	0.475	0.430	0.438	0.503	0.485	0.429	0.444	0.461	0.465
ETTh2	0.363	<u>0.393</u>	0.377	0.404	0.402	0.421	<u>0.354</u>	0.397	0.380	0.416	0.344	0.389	0.411	0.425	0.358	0.396	0.398	0.427	0.492	0.478	0.495	0.483
Weather	0.231	0.256	0.230	0.267	0.231	0.270	0.224	<u>0.262</u>	0.230	0.267	0.248	0.280	0.237	0.272	<u>0.227</u>	0.266	0.236	0.271	0.246	0.299	0.230	0.277
Traffic	0.433	<u>0.287</u>	0.468	0.336	0.420	0.284	0.430	0.300	0.525	0.382	0.462	0.330	0.463	0.335	0.444	0.316	<u>0.428</u>	0.297	0.445	0.308	0.461	0.313
Electricity	0.170	<u>0.263</u>	0.180	0.277	0.167	0.260	<u>0.170</u>	0.264	0.200	0.302	0.185	0.287	0.180	0.277	0.173	0.267	0.173	0.272	<u>0.170</u>	0.269	0.171	0.270
Wind	0.774	0.680	0.779	0.690	0.815	0.703	0.762	0.682	0.772	0.689	0.762	0.683	0.807	0.701	0.762	0.684	0.811	0.710	<u>0.744</u>	<u>0.681</u>	0.742	0.680
Solar	0.226	0.241	0.272	0.314	0.200	0.255	0.200	<u>0.253</u>	0.250	0.288	0.265	0.289	0.232	0.280	0.224	0.276	0.221	0.262	0.255	0.315	<u>0.212</u>	0.267

Table 5: Averaged forecasting results under a unified and more fair evaluation setting with a farther lookback window. Compared to Table 1, Table 5 offers a fairer comparison by adopting an extended lookback window, which better supports models like DUET and TimeFilter to realize their potential. Moreover, we fix key hyperparameters such as `d_model`, `d_ff`, learning rate, and training epochs, avoiding test-set-based tuning and ensuring a fair evaluation. See details in Appendix G and Table 21.

Ablation Experiments. We evaluate the contributions of each component in Table 2. Adaptive Patch Embedding (APE) improves performance by enabling input-aware tokenization, while segment-wise prompt tuning further enhances accuracy through localized decoding. Table 3 shows the results of different patch size combination. Figure 4 demonstrates that segmented prediction consistently outperforms non-segmented baselines, while showing robustness across different segment sizes, see details in Appendix Figure 12. We adopt a fixed segment length of $L/3$ without cherry-picking.

Main Results. As shown in Table 1, TimeMosaic consistently achieves the best or second-best performance across all benchmarks. In the more fair comparison shown in Table 5, our method also achieves competitive performance. Furthermore, TimeMosaic demonstrates robust performance under longer lookback windows, as illustrated in Figure 6. See short-term forecasting results in Appendix Table 17. Table 6 compares the best hyperparameter configurations of seven SOTA models, where all models are tuned under the same search protocol. Due to the extremely high computational cost, each model requires exploring **10,800** different

parameter settings, we only report results on seven models across five datasets.

Zero-shot. To assess cross-dataset generalization, we conduct zero-shot forecasting where models are trained on one dataset and tested on another. As shown in Appendix Table 23, TimeMosaic consistently achieves the best performance across all transfer settings, outperforming GPT4TS (Zhou et al. 2023), DLinear, and PatchTST. In addition, we further scale up TimeMosaic on the BLAST dataset (Shao et al. 2025) with an input length of 512 and an output horizon of 720. This large-scale setting (27M parameters, trained on two V100 GPUs for about 40 hours) allows a direct comparison with recent time series foundation models (TSFMs). The results (Appendix J, Tables 4 and 16) show that TimeMosaic achieves zero-shot performance on par with representative TSFMs such as TimeMoe (Shi et al. 2025), Moirai (Woo et al. 2024), Chronos (Ansari et al. 2024), TimesFM (Das et al. 2024), and Moment (Goswami et al. 2024) while maintaining a moderate model size and inference cost. This confirms that the architectural choices of adaptive patch embedding and segment-wise decoding remain effective even at the foundation-model scale.

Models	TimeMosaic		SimpleTM		TimeFilter		DUET		iTransformer		TimeMixer		PatchTST		DLinear	
	Ours		(2025)		(2025)		(2025b)		(2024a)		(2024)		(2023)		(2023)	
Metric	MSE	MAE	MSE	MAE	MSE	MAE	MSE	MAE	MSE	MAE	MSE	MAE	MSE	MAE	MSE	MAE
ETTm1	0.342	0.367	0.346	0.378	0.353	0.377	0.354	0.377	0.356	0.385	0.349	0.392	0.348	0.380	0.356	0.378
ETTm2	0.250	0.305	0.257	0.316	0.253	0.317	0.253	0.313	0.267	0.325	0.256	0.315	0.256	0.318	0.262	0.326
ETTh1	0.397	0.417	0.416	0.434	0.414	0.429	0.406	0.425	0.425	0.438	0.416	0.428	0.410	0.430	0.419	0.437
ETTh2	0.348	0.383	0.358	0.396	0.347	0.394	0.334	0.384	0.362	0.398	0.349	0.392	0.359	0.399	0.412	0.433
Weather	0.223	0.251	0.220	0.259	0.220	0.261	0.240	0.277	0.230	0.269	0.229	0.265	0.223	0.260	0.240	0.291

Table 6: Results under the hyperparameter search setting described in Appendix Section I. The lookback window is selected from $\{96, 192, 320, 512\}$, and the best configuration is reported for each model. This setup ensures that the comparison reflects each model’s optimal performance rather than a fixed setting constraint. As far as we know, we are the first open source parameter search script. See Details in Appendix Table 22.

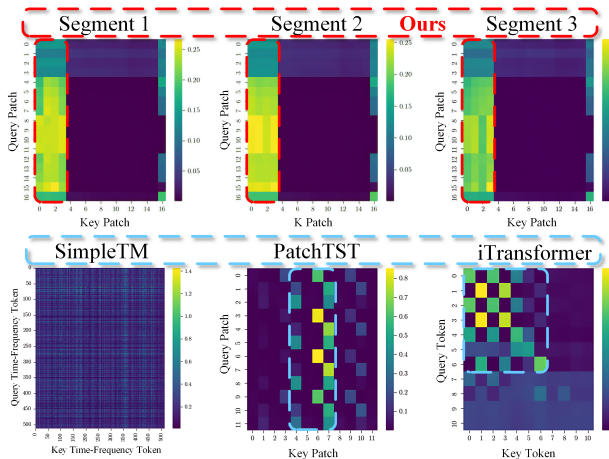


Figure 5: Attention Pattern Visualization Across Models.

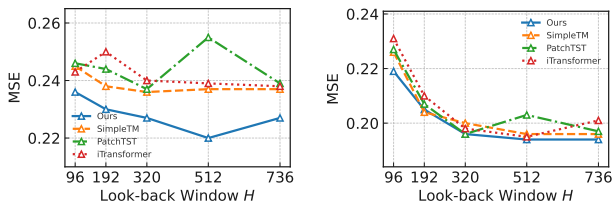


Figure 6: Sensitivity of multivariate forecasting performance to look-back window size. We evaluate four models across five input lengths ($T = 192$) on ETTm2 and Weather. See more details in Appendix G.

Efficiency Analysis. Appendix Table 15 reports forecasting error and efficiency under the unified search protocol described in Appendix Section I. For each dataset and model, we first conduct hyperparameter search and select the configuration that achieves the lowest validation error averaged over MSE and MAE. We then measure parameter count, inference latency, and GPU memory usage at this setting. This protocol anchors every method at its best attainable error level within the same search space and avoids biased comparisons that could arise from deliberately changing hy-

perparameters to influence efficiency. The results show that TimeMosaic achieves competitive or leading error on all five datasets, for example attaining the lowest MSE on ETTm2 and the lowest MAE on Weather, while keeping parameter scale in the range of a few hundred thousand, which is substantially smaller than SimpleTM or iTransformer. Although its inference time is higher than that of extremely lightweight models such as iTransformer, it remains within a reasonable margin and consistently uses moderate memory. The slightly slower inference mainly arises from the segment-wise step-by-step decoding design, and this behavior is consistent with our experimental observations. Overall, TimeMosaic presents a balanced error–efficiency performance, showing that its gains stem from architectural design rather than hyperparameter tuning.

Visualization. Existing models differ in their attention interaction schemes. PatchTST slices each variable into temporal patches and applies self-attention across patches within the same variable. iTransformer treats each variable as a token and performs self-attention across channels. In contrast, SimpleTM constructs time-frequency tokens via wavelet transforms and enables joint attention across both time and channels. Our TimeMosaic instead interacts primarily through learnable *prompt embeddings* assigned to different forecast segments, guiding the model to specialize decoding over distinct temporal intervals in Figure 5.

6 Conclusion

We proposed TimeMosaic, a forecasting framework that jointly addresses the dual challenges of encoding heterogeneity and decoding heterogeneity in multivariate time series. Through adaptive patch embedding, TimeMosaic dynamically adjusts granularity according to local information density, ensuring both motif reuse and structural clarity while maintaining temporal coherence. Complementarily, segment-wise prompt tuning enables horizon-aware forecasting by treating different prediction segments as related subtasks within a unified multi-task paradigm. Extensive experiments verify that TimeMosaic achieves consistent improvements in forecasting accuracy and efficiency. In future work, we will extend TimeMosaic to streaming scenarios and investigate its potential for large-scale pretraining towards time series foundation modeling.

Acknowledgments

This research was partly supported by the National Natural Science Foundation of China under Grant Nos. U24A20232 and 62402475.

References

- Ansari, A. F.; Stella, L.; Turkmen, C.; Zhang, X.; Mercado, P.; Shen, H.; Shchur, O.; Rangapuram, S. S.; Pineda Arango, S.; Kapoor, S.; Zschiegner, J.; Maddix, D. C.; Mahoney, M. W.; Torkkola, K.; Gordon Wilson, A.; Bohlke-Schneider, M.; and Wang, Y. 2024. Chronos: Learning the Language of Time Series. *Transactions on Machine Learning Research (TMLR)*.
- Axtell, R. L. 2001. Zipf Distribution of U.S. Firm Sizes. *Science*, 293(5536): 1818–1820.
- Cao, J.; Li, J.; Yang, Z.; and Zhou, R. 2024. Enhanced Multimodal Aspect-Based Sentiment Analysis by LLM-Generated Rationales. In *International Conference on Neural Information Processing*, 228–243. Springer.
- Chen, H.; Luong, V.; Mukherjee, L.; and Singh, V. 2025. SimpleTM: A Simple Baseline for Multivariate Time Series Forecasting. In *The Thirteenth International Conference on Learning Representations*.
- Chen, P.; Zhang, Y.; Cheng, Y.; Shu, Y.; Wang, Y.; Wen, Q.; Yang, B.; and Guo, C. 2024. Pathformer: Multi-scale Transformers with Adaptive Pathways for Time Series Forecasting. In *International Conference on Learning Representations (ICLR)*.
- Crawshaw, M. 2020a. Multi-Task Learning with Deep Neural Networks: A Survey.
- Crawshaw, M. 2020b. Multi-Task Learning with Deep Neural Networks: A Survey. *CoRR*, abs/2009.09796.
- Das, A.; Kong, W.; Sen, R.; and Zhou, Y. 2024. A decoder-only foundation model for time-series forecasting. In *Proceedings of the 41st International Conference on Machine Learning (ICML)*.
- Ding, K.; Fan, F.; Wang, Y.; Jian, R.; Wang, X.; Gong, L.; Jiang, Y.; Luo, C.; and Zhan, J. 2025. DualSG: A Dual-Stream Explicit Semantic-Guided Multivariate Time Series Forecasting Framework. In *Proceedings of the 33rd ACM International Conference on Multimedia*.
- Emami, P.; Sahu, A.; and Graf, P. 2023. BuildingsBench: A Large-Scale Dataset of 900K Buildings and Benchmark for Short-Term Load Forecasting. In *Thirty-seventh Conference on Neural Information Processing Systems Datasets and Benchmarks Track*.
- Eyring, V.; Bony, S.; Meehl, G. A.; Senior, C. A.; Stevens, B.; Stouffer, R. J.; and Taylor, K. E. 2016. Overview of the Coupled Model Intercomparison Project Phase 6 (CMIP6) experimental design and organization. *Geoscientific Model Development*, 9(5): 1937–1958.
- Goswami, M.; Szafer, K.; Choudhry, A.; Cai, Y.; Li, S.; and Dubrawski, A. 2024. MOMENT: A Family of Open Time-series Foundation Models. In *International Conference on Machine Learning (ICML)*.
- Hersbach, H.; Bell, B.; Berrisford, P.; Hirahara, S.; Horányi, A.; Muñoz-Sabater, J.; Nicolas, J.; Peubey, C.; Radu, R.; Schepers, D.; Simmons, A.; Soci, C.; Abdalla, S.; Abellan, X.; Balsamo, G.; Bechtold, P.; Biavati, G.; Bidlot, J.; Bonavita, M.; De Chiara, G.; Dahlgren, P.; Dee, D.; Diamantakis, M.; Dragani, R.; Flemming, J.; Forbes, R.; Fuentes, M.; Geer, A.; Haimberger, L.; Healy, S.; Hogan, R. J.; Hólm, E.; Janisková, M.; Keeley, S.; Laloyaux, P.; Lopez, P.; Lupu, C.; Radnoti, G.; de Rosnay, P.; Rozum, I.; Vamborg, F.; Villaume, S.; and Thépaut, J.-N. 2020. The ERA5 global reanalysis. *Quarterly Journal of the Royal Meteorological Society*, 146(730): 1999–2049.
- Hu, Y.; Zhang, G.; Liu, P.; Lan, D.; Li, N.; Cheng, D.; Dai, T.; Xia, S.-T.; and Pan, S. 2025. TimeFilter: Patch-Specific Spatial-Temporal Graph Filtration for Time Series Forecasting. In *International Conference on Machine Learning*.
- Huang, M.; Mao, Z.; Chen, Z.; and Zhang, Y. 2023. Towards Accurate Image Coding: Improved Autoregressive Image Generation With Dynamic Vector Quantization. In *Proceedings of the IEEE/CVF Conference on Computer Vision and Pattern Recognition (CVPR)*, 22596–22605.
- Huang, Q.; Zhou, Z.; Yang, K.; Yi, Z.; Wang, X.; Jiang, W.; and Wang, Y. 2025. TimeBase: The Power of Minimalism in Long-term Time Series Forecasting. In *International Conference on Learning Representations (ICLR)*.
- Jang, E.; Gu, S.; and Poole, B. 2017. Categorical Reparameterization with Gumbel-Softmax. *arXiv preprint arXiv:1611.01144*.
- Jin, M.; Wang, S.; Ma, L.; Chu, Z.; Zhang, J. Y.; Shi, X.; Chen, P.-Y.; Liang, Y.; Li, Y.-F.; Pan, S.; and Wen, Q. 2024. Time-LLM: Time Series Forecasting by Reprogramming Large Language Models. In *International Conference on Learning Representations (ICLR)*.
- Khalidi, R.; El Afia, A.; Chiheb, R.; and Tabik, S. 2023. What is the best RNN-cell structure to forecast each time series behavior? *Expert Systems with Applications*, 215: 119140.
- Kim, T.; Kim, J.; Tae, Y.; Park, C.; Choi, J.-H.; and Choo, J. 2021. Reversible Instance Normalization for Accurate Time-Series Forecasting against Distribution Shift. In *International Conference on Learning Representations*.
- Kong, Y.; Wang, Z.; Nie, Y.; Zhou, T.; Zohren, S.; Liang, Y.; Sun, P.; and Wen, Q. 2025. Unlocking the Power of LSTM for Long Term Time Series Forecasting. In *Proceedings of the AAAI Conference on Artificial Intelligence*.
- Kudrat, D.; Xie, Z.; Sun, Y.; Jia, T.; and Hu, Q. 2025. Patchwise Structural Loss for Time Series Forecasting. In *ICML*.
- Laban, P.; Kryscinski, W.; Agarwal, D.; Fabbri, A.; Xiong, C.; Joty, S.; and Wu, C.-S. 2023. SummEdits: Measuring LLM Ability at Factual Reasoning Through The Lens of Summarization. In *EMNLP*.
- Lai, G.; Chang, W.-C.; Yang, Y.; and Liu, H. 2018. Modeling Long- and Short-Term Temporal Patterns with Deep Neural Networks. In *ACM SIGIR*.
- Lester, B.; Al-Rfou, R.; and Constant, N. 2021. The Power of Scale for Parameter-Efficient Prompt Tuning. In *EMNLP*.

- Lin, S.; Lin, W.; Wu, W.; Zhao, F.; Mo, R.; and Zhang, H. 2023. Segrnn: Segment recurrent neural network for long-term time series forecasting. *arXiv preprint arXiv:2308.11200*.
- Liu, H.; Ma, Z.; Yang, L.; Zhou, T.; Xia, R.; Wang, Y.; Wen, Q.; and Sun, L. 2023. SADI: A Self-Adaptive Decomposed Interpretable Framework for Electric Load Forecasting Under Extreme Events. In *IEEE International Conference on Acoustics, Speech and Signal Processing*.
- Liu, X.; Zheng, Y.; Du, Z.; Ding, M.; Qian, Y.; Yang, Z.; and Tang, J. 2021. GPT Understands, Too. *arXiv:2103.10385*.
- Liu, Y.; Hu, T.; Zhang, H.; Wu, H.; Wang, S.; Ma, L.; and Long, M. 2024a. iTransformer: Inverted Transformers Are Effective for Time Series Forecasting. In *International Conference on Learning Representations (ICLR)*.
- Liu, Y.; Qin, G.; Shi, Z.; Chen, Z.; Yang, C.; Huang, X.; Wang, J.; and Long, M. 2025. Sundial: A Family of Highly Capable Time Series Foundation Models. In *International Conference on Machine Learning*.
- Liu, Y.; Zhang, H.; Li, C.; Huang, X.; Wang, J.; and Long, M. 2024b. Timer: Generative Pre-trained Transformers Are Large Time Series Models. In *Forty-first International Conference on Machine Learning*.
- Morid, M. A.; Sheng, O. R. L.; and Dunbar, J. 2023. Time Series Prediction Using Deep Learning Methods in Healthcare. *ACM Trans. Manage. Inf. Syst.*, 14.
- Nate Gruver, S. Q., Marc Finzi, and Wilson, A. G. 2023. Large Language Models Are Zero Shot Time Series Forecasters. In *Advances in Neural Information Processing Systems*.
- Nie, Y.; Nguyen, N. H.; Sinthong, P.; and Kalagnanam, J. 2023. A Time Series is Worth 64 Words: Long-term Forecasting with Transformers. In *International Conference on Learning Representations (ICLR)*.
- Paszke, A.; Gross, S.; Massa, F.; Lerer, A.; Bradbury, J.; Chanan, G.; Killeen, T.; Lin, Z.; Gimelshein, N.; Antiga, L.; Desmaison, A.; Köpf, A.; Yang, E.; DeVito, Z.; Raison, M.; Tejani, A.; Chilamkurthy, S.; Steiner, B.; Fang, L.; Bai, J.; and Chintala, S. 2019. PyTorch: An Imperative Style, High-Performance Deep Learning Library.
- Qiu, X.; Hu, J.; Zhou, L.; Wu, X.; Du, J.; Zhang, B.; Guo, C.; Zhou, A.; Jensen, C. S.; Sheng, Z.; and Yang, B. 2024. TFB: Towards Comprehensive and Fair Benchmarking of Time Series Forecasting Methods. *Proc. VLDB Endow.*, 17(9): 2363–2377.
- Qiu, X.; Wu, X.; Cheng, H.; Liu, X.; Guo, C.; Hu, J.; and Yang, B. 2025a. DBLoss: Decomposition-based Loss Function for Time Series Forecasting. In *NeurIPS*.
- Qiu, X.; Wu, X.; Lin, Y.; Guo, C.; Hu, J.; and Yang, B. 2025b. DUET: Dual Clustering Enhanced Multivariate Time Series Forecasting. In *SIGKDD*, 1185–1196.
- Qiu, X.; Zhu, Y.; Li, Z.; Cheng, H.; Wu, X.; Guo, C.; Yang, B.; and Hu, J. 2025c. DAG: A dual causal network for time series forecasting with exogenous variables. *arXiv preprint arXiv:2509.14933*.
- Ranzato, M.; Chopra, S.; Auli, M.; and Zaremba, W. 2016. Sequence Level Training with Recurrent Neural Networks. arXiv:1511.06732.
- Rasp, S.; Dueben, P. D.; Scher, S.; Weyn, J. A.; Mouatadid, S.; and Thuerey, N. 2020. WeatherBench: A Benchmark Data Set for Data-Driven Weather Forecasting. *Journal of Advances in Modeling Earth Systems*, 12(11): e2020MS002203.
- Rousseeuw, P. J. 1987. Silhouettes: A graphical aid to the interpretation and validation of cluster analysis. *Journal of Computational and Applied Mathematics*, 20: 53–65.
- Ruder, S. 2017. An Overview of Multi-Task Learning in Deep Neural Networks. arXiv:1706.05098.
- Schneider, S. H.; and Dickinson, R. E. 1974. Climate modeling. *Reviews of Geophysics*, 12(3): 447–493.
- Shao, Z.; Li, Y.; Wang, F.; Yu, C.; Fu, Y.; Qian, T.; Xu, B.; Diao, B.; Xu, Y.; and Cheng, X. 2025. BLAST: Balanced Sampling Time Series Corpus for Universal Forecasting Models. In *Proceedings of the 31st ACM SIGKDD Conference on Knowledge Discovery and Data Mining V.2*.
- Shi, X.; Wang, S.; Nie, Y.; Li, D.; Ye, Z.; Wen, Q.; and Jin, M. 2025. Time-MoE: Billion-Scale Time Series Foundation Models with Mixture of Experts. In *International Conference on Learning Representations (ICLR)*.
- Shu, W.; Cai, K.; and Xiong, N. N. 2021. A short-term traffic flow prediction model based on an improved gate recurrent unit neural network. *IEEE Transactions on Intelligent Transportation Systems*, 23(9): 16654–16665.
- Stankeviciute, K.; M Alaa, A.; and Van der Schaar, M. 2021. Conformal time-series forecasting. *Advances in neural information processing systems*, 34: 6216–6228.
- Stitsyuk, A.; and Choi, J. 2025. xPatch: Dual-Stream Time Series Forecasting with Exponential Seasonal-Trend Decomposition. In *Proceedings of the AAAI Conference on Artificial Intelligence*.
- Tang, P.; and Zhang, W. 2025. Unlocking the Power of Patch: Patch-Based MLP for Long-Term Time Series Forecasting. In *AAAI*.
- Wang, H.; Pan, L.; Chen, Z.; Yang, D.; Zhang, S.; Yang, Y.; Liu, X.; Li, H.; and Tao, D. 2025a. FreDF: Learning to Forecast in the Frequency Domain. In *ICLR*.
- Wang, S.; Li, J.; Shi, X.; Ye, Z.; Mo, B.; Lin, W.; Ju, S.; Chu, Z.; and Jin, M. 2025b. TimeMixer++: A General Time Series Pattern Machine for Universal Predictive Analysis. In *International Conference on Learning Representations (ICLR)*.
- Wang, S.; Wu, H.; Shi, X.; Hu, T.; Luo, H.; Ma, L.; Zhang, J. Y.; and ZHOU, J. 2024. TimeMixer: Decomposable Multiscale Mixing for Time Series Forecasting. In *International Conference on Learning Representations (ICLR)*.
- Warren Liao, T. 2005. Clustering of time series data—a survey. *Pattern Recognition*, 38(11): 1857–1874.
- Woo, G.; Liu, C.; Kumar, A.; Xiong, C.; Savarese, S.; and Sahoo, D. 2024. Unified Training of Universal Time Series Forecasting Transformers. In *Forty-first International Conference on Machine Learning (ICML)*.

- Wu, H.; Hu, T.; Liu, Y.; Zhou, H.; Wang, J.; and Long, M. 2023. TimesNet: Temporal 2D-Variation Modeling for General Time Series Analysis. In *International Conference on Learning Representations*.
- Xia, Y.; Fu, F.; Zhang, W.; Jiang, J.; and Cui, B. 2024. Efficient Multi-task LLM Quantization and Serving for Multiple LoRA Adapters. In *Advances in Neural Information Processing Systems*.
- Xie, Y.; Xiong, Y.; Shi, Z.; Niu, H.; and Liu, Z. 2025. The language of time: a language model perspective on time-series foundation models.
- Yadav, H.; and Thakkar, A. 2024. NOA-LSTM: An efficient LSTM cell architecture for time series forecasting. *Expert Systems with Applications*, 238: 122333.
- Yi, K.; Zhang, Q.; Fan, W.; Wang, S.; Wang, P.; He, H.; An, N.; Lian, D.; Cao, L.; and Niu, Z. 2023. Frequency-domain MLPs are More Effective Learners in Time Series Forecasting. In *Advances in Neural Information Processing Systems*.
- Yu, C.; Wang, F.; Shao, Z.; Qian, T.; Zhang, Z.; Wei, W.; and Xu, Y. 2024. Ginar: An end-to-end multivariate time series forecasting model suitable for variable missing. In *SIGKDD*.
- Yu, C.; Wang, F.; Shao, Z.; Sun, T.; Wu, L.; and Xu, Y. 2023. DSformer: A Double Sampling Transformer for Multivariate Time Series Long-term Prediction. In *CIKM*.
- Zeng, A.; Chen, M.; Zhang, L.; and Xu, Q. 2023. Are Transformers Effective for Time Series Forecasting? In *Proceedings of the AAAI Conference on Artificial Intelligence*.
- Zhang, T.; Zhang, Y.; Cao, W.; Bian, J.; Yi, X.; Zheng, S.; and Li, J. 2022. Less Is More: Fast Multivariate Time Series Forecasting with Light Sampling-oriented MLP Structures. *arXiv:2207.01186*.
- Zhang, W.; Deng, Y.; Liu, B.; Pan, S.; and Bing, L. 2024. Sentiment Analysis in the Era of Large Language Models: A Reality Check. In *NAACL*.
- Zheng, W.; Zhao, P.; Chen, G.; Zhou, H.; and Tian, Y. 2023. A Hybrid Spiking Neurons Embedded LSTM Network for Multivariate Time Series Learning Under Concept-Drift Environment. *IEEE Trans. Knowl. Data Eng.*, 35(7): 6561–6574.
- Zhou, H.; Zhang, S.; Peng, J.; Zhang, S.; Li, J.; Xiong, H.; and Zhang, W. 2021. Informer: Beyond Efficient Transformer for Long Sequence Time-Series Forecasting. In *Proceedings of the AAAI Conference on Artificial Intelligence*.
- Zhou, T.; Niu, P.; Wang, X.; Sun, L.; and Jin, R. 2023. One Fits All: Power General Time Series Analysis by Pretrained LM. In *Advances in Neural Information Processing Systems*.
- Zhu, P.; Li, Y.; Hu, Y.; Liu, Q.; Cheng, D.; and Liang, Y. 2024a. LSR-IGRU: Stock Trend Prediction Based on Long Short-Term Relationships and Improved GRU. *International Conference on Information and Knowledge Management*.
- Zhu, P.; Li, Y.; Hu, Y.; Xiang, S.; Liu, Q.; Cheng, D.; and Liang, Y. 2024b. MCI-GRU: Stock Prediction Model Based on Multi-Head Cross-Attention and Improved GRU. *arXiv preprint arXiv:2410.20679*.
- Zhuang, Y.; Yu, Y.; Wang, K.; Sun, H.; and Zhang, C. 2023. ToolQA: A Dataset for LLM Question Answering with External Tools. In *Advances in Neural Information Processing Systems*.

Appendix

A Experiment Details

Datasets. We evaluate our model on a total of **seventeen** real-world multivariate time series datasets, covering both **long-term** and **short-term** forecasting tasks. The datasets span diverse domains including electricity, weather, traffic, and renewable energy, ensuring the robustness and generality of our approach. Details are as follows:

- **Electricity Transformer Temperature (ETT)**¹: Consists of four subsets. ETTh1 and ETTh2 are recorded hourly, while ETTm1 and ETTm2 are recorded every 15 minutes. The data is collected from two different electric transformers.
- **Weather**²: Contains 21 meteorological indicators collected every 10 minutes in Germany in 2020, from the Weather Station of the Max Planck Biogeochemistry Institute.
- **Traffic**³: Hourly road occupancy rates recorded by 862 sensors on freeways in the San Francisco Bay Area from January 2015 to December 2016.
- **Electricity**⁴: Hourly electricity consumption data from 321 clients spanning the period from 2012 to 2014.
- **Exchange-rate**⁵: Daily exchange rates of 8 countries from 1990 to 2016.
- **Solar-energy**⁶: 10-minute solar power production records from 137 photovoltaic plants throughout 2006.
- **Wind**⁷: Wind power and meteorological measurements collected from four real-world wind farm locations. The dataset includes hourly wind speed and power generation data, designed for wind power forecasting tasks.
- **PEMS**⁸: The PEMS datasets are designed for short-term forecasting and contain high-frequency traffic measurements at multiple locations. It includes four subsets: PEMS03, PEMS04, PEMS07, and PEMS08, with 5-minute sampling intervals and varying spatial dimensions (number of sensors).

Forecasting Settings. In accordance with prior works such as (Wu et al. 2023), we adopt prediction lengths of {96, 192, 336, 720} for long-term forecasting tasks, and a fixed length of 12 for short-term forecasting. However, we identify a common experimental flaw: the test data loader in these works often sets `drop_last=True`, which may discard up to `batch.size - 1` samples during evaluation. This issue has been discussed in (Qiu et al. 2024), yet persists in recent literature (Chen et al. 2025; Wang et al.

2025a). To ensure fair comparison and full test coverage, we uniformly set `drop_last=False` in our experiments.

Table 7 summarizes the statistics of all datasets used.

Dataset	Dim	Dataset Size	Frequency
ETTh1,ETTh2	7	(8545,2881,2881)	Hourly
ETTm1,ETTm2	7	(34465,11521,11521)	15 min
Weather	21	(36792,5271,10540)	10 min
Traffic	862	(12185,1757,3509)	Hourly
Electricity	321	(18317,2633,5261)	Hourly
Exchange-rate	8	(5120,665,1422)	Daily
Solar-energy	137	(36792,5271,10540)	10 min
Wind	9	(30468,4286,8665)	Hourly
PEMS03	358	(15617,5135,5135)	5 min
PEMS04	307	(10172,3375,3375)	5 min
PEMS07	883	(16911,5622,5622)	5 min
PEMS08	170	(10690,3548,265)	5 min

Table 7: Detailed dataset descriptions. Dim denotes dimension, which is the variate number of each dataset. Dataset size denotes the total number of time points in (Train, Validation, Test) split. Frequency denotes the sampling interval of time points.

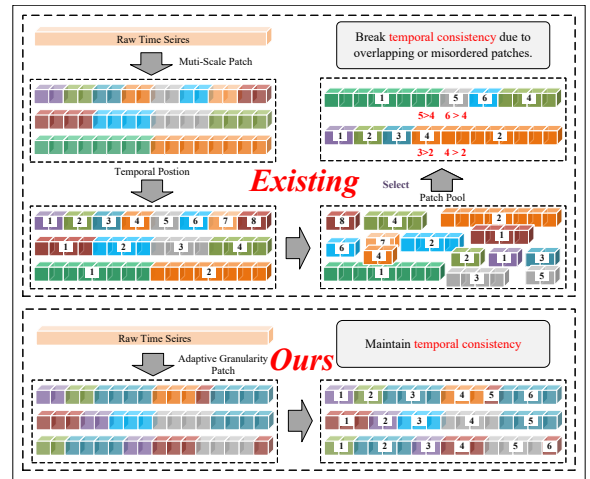


Figure 7: Comparison between existing multi-granularity patching methods and our approach. Previous methods may disrupt temporal order by inserting coarse and fine patches out of sequence, whereas our method ensures strict chronological alignment with adaptive patch sizes.

B Construction of Patch Transition Matrix

To visualize sequential dependencies among temporal patches, we construct a patch-level transition probability matrix based on clustered patch assignments. The procedure is as follows:

Patch extraction. We collect a large-scale corpus of multivariate time series forecasting datasets (see Appendix A for full dataset list). For each univariate channel, we normalize the values using min-max scaling and segment the

¹<https://github.com/zhouhaoyi/ETDataset>

²<https://www.bgc-jena.mpg.de/wetter>

³<https://pems.dot.ca.gov>

⁴<https://archive.ics.uci.edu/dataset/321/electricityloaddiagrams20112014>

⁵<https://github.com/laiquokun/multivariate-time-series-data>

⁶<https://www.nrel.gov/grid/solar-power-data.html>

⁷<https://www.kaggle.com/datasets/mubashirrahim/wind-power-generation-data-forecasting>

⁸<https://pems.dot.ca.gov/>

sequence into non-overlapping fixed-length patches of size P (set to 16 by default). This yields a collection of patch vectors $\{\mathbf{x}_i \in \mathbb{R}^P\}_{i=1}^N$ extracted from diverse domains.

Patch quantization. We apply K-Means clustering to the patch collection to obtain a discrete tokenization of the continuous patch space. Each patch \mathbf{x}_i is assigned to one of K clusters, resulting in a token sequence $\{t_i \in \{1, \dots, K\}\}_{i=1}^N$.

Transition matrix computation. We define a transition matrix $\mathbf{C} \in \mathbb{N}^{K \times K}$ where $\mathbf{C}_{i,j}$ counts the number of times a patch of cluster i is immediately followed by a patch of cluster j in the tokenized sequence. The row-normalized transition probability matrix $\mathbf{P} \in [0, 1]^{K \times K}$ is then computed as:

$$\mathbf{P}_{i,j} = \frac{\mathbf{C}_{i,j}}{\sum_{j'} \mathbf{C}_{i,j'} + \epsilon}$$

where ϵ is a small constant to avoid division by zero.

Visualization. We identify the top- k most frequent patch clusters based on row-wise sums of \mathbf{C} and extract the corresponding $k \times k$ submatrix from \mathbf{P} . This submatrix is visualized using a heatmap (Figure 2, where high-probability transitions indicate strong sequential dependencies between dominant patch types).

Implementation. The full construction and visualization pipeline is implemented in Python using `scikit-learn`, `seaborn`, and `matplotlib`. The source code is included in our supplementary materials. The key parameters are set to $P = 16$, $K = 100$, and $k = 20$ in our default configuration.

C Patch Granularity Selection.

Figure 9 and Figure 8 compare the distribution of selected patch sizes under different look-back windows across four datasets (ETTh1, ETTh2, ETTm1, and ETTm2), with and without the proposed *budget* strategy, respectively. Without the budget constraint (Figure 8), the model exhibits a clear tendency to select coarse-grained patches, with `Patch 32` dominating across all settings. In contrast, the budget-aware variant (Figure 9) promotes a more balanced selection across all three patch sizes, indicating that the budget loss effectively encourages granularity diversity and prevents overuse of coarse patterns.

Figure 10 shows the Zipf deviation (top) and Silhouette score (bottom) across different patch granularities (8, 16, 32, and `Mixed`) under varying numbers of clusters. These metrics are computed after applying PCA projection and k -means clustering on patch representations. We observe a clear trade-off: finer patches (e.g., `Patch 8`) exhibit better structural clarity (higher Silhouette score) but lower pattern reuse (higher Zipf deviation), while coarser patches (e.g., `Patch 32`) show better reuse but less cluster cohesion. The `Mixed` configuration balances both objectives by projecting patches of different granularities into a shared space before clustering, achieving a favorable compromise between diversity and structural consistency.

Quantitative Analysis. Table 8 reports the Zipf deviation and Silhouette scores under various patch sizes and cluster configurations. Finer-grained patches (e.g., size 8) exhibit clearer clustering structure (higher Silhouette scores) but reduced pattern reuse (higher Zipf deviation), while coarser patches (e.g., size 64) show the opposite trend. Notably, the `Mixed` configuration, which merges patches of size 8, 16, and 32, achieves a favorable balance between diversity and structural clarity, further supporting the effectiveness of patch granularity mixing.

Patch Size	Global Patches	Clusters (C)	Silhouette	Zipf Deviation
8	152,418	16	0.2978	0.4853
		32	0.2392	0.5678
		48	0.2073	0.6301
16	76,202	16	0.2717	0.5804
		32	0.2188	0.6856
		48	0.1845	0.6749
32	38,094	16	0.2454	0.6066
		32	0.1783	0.7204
		48	0.1623	0.7529
64	19,040	16	0.2115	0.6896
		32	0.1862	0.7597
		48	0.1547	0.7530
Mixed	266,714	16	0.2913	0.7171
		32	0.2491	0.6844
		48	0.2021	0.7147

Table 8: Zipf deviation and Silhouette score across different patch granularities and cluster sizes. (ETT Datasets)

D Channel Modeling Variants

To support multivariate time series forecasting, our framework incorporates a modular *channel modeling interface* that controls how variables interact before temporal encoding. While the main paper adopts the `CI+` strategy by default, we provide several alternative implementations, which can be flexibly selected based on the correlation structure of the dataset. All variants generate an auxiliary token sequence `extra_token` to be concatenated with the patch sequence for each variable before encoding.

CI (Channel-Independent): Each variable is modeled independently by reshaping the input $x \in \mathbb{R}^{B \times T \times C}$ to $[B \cdot C, T]$, and computing patch embeddings separately. No information is shared across variables.

CD-G (Channel-Dependent with Global Token): The mean signal across all variables is pooled to generate a global context token, which is broadcast to all variable streams and prepended to their patch embeddings.

CD-P (Channel-Dependent Plus). An enhanced channel-dependent modeling strategy that incorporates timestamp (time feature) information into inter-channel interactions. Unlike `CI` or basic `CD` designs, `CD-P` explicitly injects temporal encoding (e.g., positional or calendar time) into

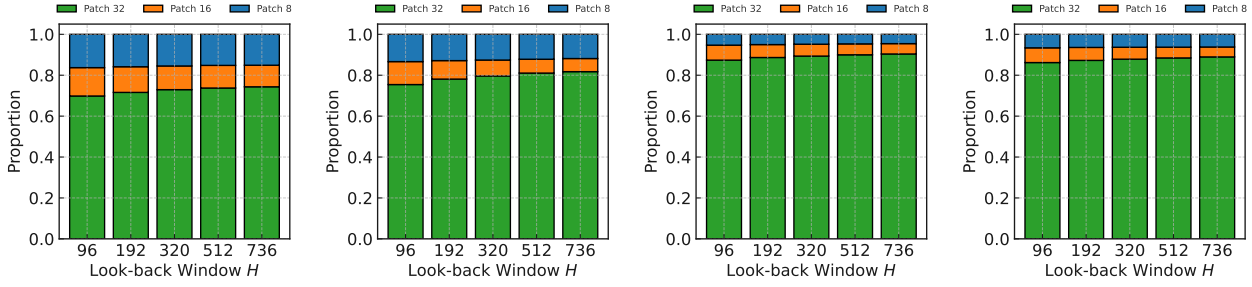


Figure 8: No budget strategy. Segments of different sizes on different dataset with a predicted length of 192. From left to right the datasets are ETTh1, ETTh2, ETTm1 and ETTm2.

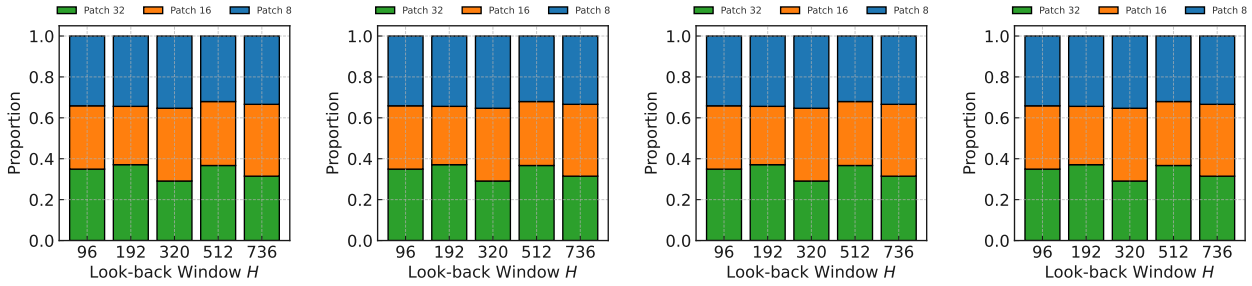


Figure 9: Segments of different sizes on different dataset with a predicted length of 192. From left to right the datasets are ETTh1, ETTh2, ETTm1 and ETTm2.

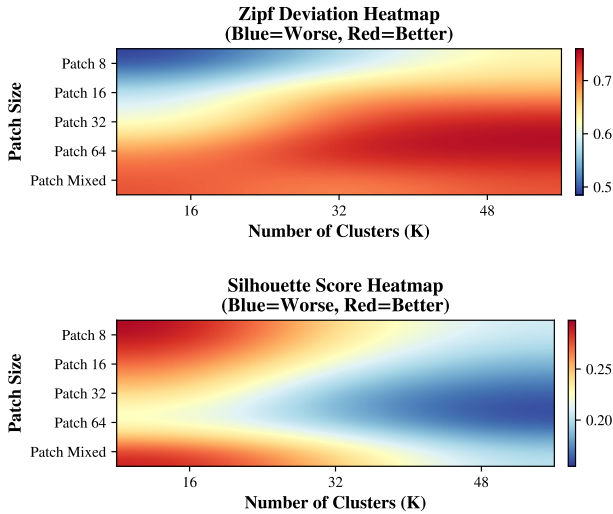


Figure 10: Zipf deviation and Silhouette score with Patch Mixed.

each variable’s representation, facilitating temporally aware cross-channel modeling.

CD-A (Channel-Dependent with Calendar-Aware Prompts): Time encoding features (e.g., timestamps, day-of-week) are embedded to generate calendar-aware prompt tokens shared across all variables. This variant is

especially effective in periodic domains.

CI+ (Channel-Independent with Prompt Conditioning): Combines the advantages of CI with prompt-based guidance: each variable retains its independence but is augmented with its own channel token and K global prompt tokens. This hybrid design preserves robustness while introducing controllable task-level bias.

Usage Notes. All variants are plug-and-play, require minimal code change, and share the same forecasting backbone. In our experiments, CI+ consistently offers a good balance between performance and stability across diverse datasets, especially when variable correlation is moderate or unknown.

Ablation Results. Table 9 compares five channel modeling strategies on ETTh2 and Weather datasets under a unified backbone and training protocol. CI+ achieves the best or near-best performance on both datasets, validating the benefit of shared channel interaction. Notably, CD-P and CD-A perform more competitively on the Weather dataset, which contains 21 variables (vs. 7 in ETTh2), indicating that richer inter-variable relationships allow channel-dependent strategies to better exploit temporal or global correlations.

Notes Experiment Setting. In Table 20, we search over several channel modeling strategies and report the best-performing configuration, while in Table 21, we fix the channel-independent setting for all models.

Method	ETTh2				Weather			
	96	192	336	720	96	192	336	720
CI	0.295	0.380	0.421	0.425	0.178	0.223	0.281	0.358
CI+	0.291	0.375	0.425	0.415	0.170	0.221	0.276	0.354
CDG	0.299	0.395	0.427	0.444	0.174	0.222	0.280	0.357
CDP	0.292	0.377	0.425	0.425	0.169	0.222	0.279	0.357
CDA	0.297	0.375	0.429	0.424	0.173	0.218	0.276	0.355

Table 9: Ablation of channel modeling strategies (MSE) on two representative datasets.

E Benchmark Implementation

To ensure a comprehensive and fair evaluation, we have implemented a broad suite of representative time series forecasting models within a unified benchmarking framework. Our benchmark includes 30+ models spanning diverse architectural paradigms, such as Transformer-based, MLP-based, and hybrid designs.

Specifically, our benchmark covers mainstream Transformer-based models including PatchTST, iTransformer, SimpleTM, TimesNet, TimeMixer, TimeMixer++, Informer, Autoformer, FEDformer, Pyraformer, Reformer, ETSformer, Crossformer, TiDE, SCINet, MICN, and SegRNN. These models capture various design philosophies such as decomposition, frequency-domain modeling, inverted attention, and non-stationary transformation.

We also include lightweight and MLP-based approaches such as DLinear, LightTS, TSMixer, PatchMLP, xPatch, and TimeFilter, which emphasize efficiency and simplicity over architectural complexity.

In addition, we integrate several recently proposed hybrid and multi-resolution models, including DUET, PathFormer, FreTS, and WPMixer, to assess the effectiveness of multi-scale temporal modeling strategies.

Finally, our own method, TimeMosaic, is evaluated under the same pipeline. All models share consistent training protocols, data loading procedures, and evaluation metrics. This unified implementation allows for a rigorous and reproducible comparison across a diverse range of baselines.

Discussion on the Unified Benchmark Setting. All experimental results reported in this paper are based on our own constructed unified benchmark, where we deliberately avoided over-tuning hyperparameters and fixed them consistently across models. It is therefore understandable that our reported results differ from those in original papers. However, this difference does not imply that the results in other papers are incorrect or unreliable; rather, it simply reflects performance under our more strictly controlled and unified evaluation setting. Currently, there remains debate within the community regarding the fairness of this approach: one perspective argues that unified hyperparameter settings provide a fairer basis for comparison, while another contends that certain models require specific hyperparameter choices to achieve convergence or optimal performance. Investigating this trade-off comprehensively is an important direction for our future research.

Dataset	TimeMosaic	SimpleTM	PatchTST	Improve vs ST	Improve vs PT
ETTm1	0.381	0.403	0.398	+5.45%	+4.27%
ETTm2	0.314	0.325	0.323	+3.38%	+2.79%
ETTh1	0.424	0.436	0.431	+2.75%	+1.63%
ETTh2	0.388	0.413	0.402	+6.06%	+3.48%
Weather	0.267	0.282	0.283	+5.32%	+5.65%
Traffic	0.283	0.347	0.314	+18.45%	+9.87%
Electricity	0.279	0.284	0.292	+1.76%	+4.45%
Exchange	0.403	0.411	0.401	+1.95%	-0.50%
Solar	0.270	0.333	0.397	+18.92%	+32.00%
Average	—	—	—	+7.12%	+7.07%

Table 10: Per-dataset MAE and relative improvement of TimeMosaic over SimpleTM (ST) and PatchTST (PT).

F Statistical Significance Analysis

To evaluate the statistical significance of our model’s improvements, we compare TimeMosaic against two baselines, SimpleTM and PatchTST, on the 9 benchmark datasets using the MAE metric. For each dataset, we report the MAE values and compute the relative improvement of TimeMosaic over each baseline. Furthermore, we conduct Wilcoxon signed-rank tests to assess whether the improvements are statistically significant.

We further perform Wilcoxon signed-rank tests to assess the significance of these improvements. The results confirm that the improvements are statistically significant:

- TimeMosaic vs SimpleTM: $p = 0.00195$
- TimeMosaic vs PatchTST: $p = 0.00391$

These results demonstrate that TimeMosaic consistently and significantly outperforms strong baselines across datasets under the MAE metric.

G Detailed Results

In accordance with prior works such as (Wu et al. 2023), we adopt the standard prediction lengths of {96, 192, 336, 720} for long-term forecasting tasks, and a fixed length of 12 for short-term forecasting.

Drop Last. We further identify a common experimental flaw in many recent works: the test dataloader is often configured with `drop_last=True`, which can silently discard up to `batch_size - 1` samples during evaluation. Although this issue has been highlighted in (Qiu et al. 2024), it remains present in recent literature (Chen et al. 2025; Wang et al. 2025a). To address this, we explicitly set `drop_last=False` in all our evaluations, ensuring complete coverage of the test set.

Over-tuning hyperparameters. Moreover, we observe that several recent methods rely on overly aggressive hyperparameter tuning strategies, such as assigning distinct learning rates to each forecasting length (e.g., $lr = \{2.42 \times 10^{-4}, 2.01 \times 10^{-4}, 1.32 \times 10^{-4}, 2.39 \times 10^{-4}\}$ for $T = \{96, 192, 336, 720\}$) or customizing hyperparameters for each dataset. Such practices inflate performance but undermine comparability. In contrast, we use consistent settings across horizons and datasets unless explicitly stated, thereby ensuring a level playing field for all methods evaluated.

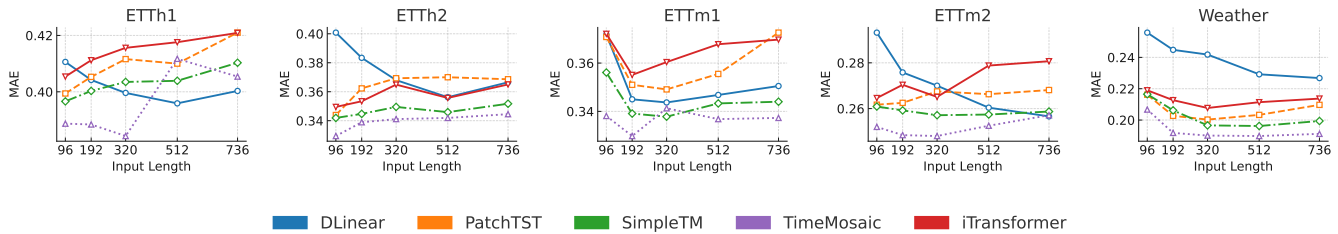


Figure 11: MAE performance across different input lengths for five benchmark datasets. Each subplot compares five models under varying look-back windows.

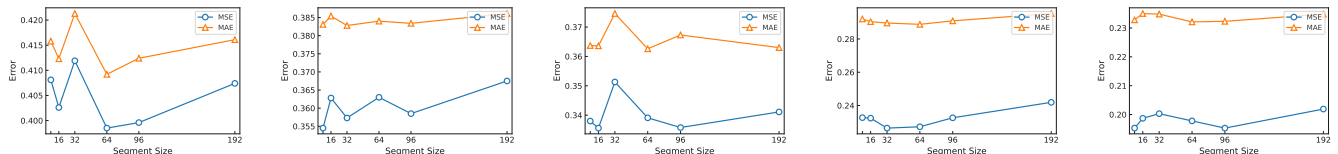


Figure 12: Segments of different sizes on five datasets with a predicted length of 192. Each figure presents both MSE and MAE performance curves across different segment sizes.

Details Results. Table 20 and Table 21 presents the complete results of long-term forecasting. Table 23 shows the results of zero-shot prediction. As shown in Table 13, to ensure fairness and robust performance across datasets, we choose the patch granularity [8, 16, 32] as a representative configuration for all subsequent experiments.

Lookback Windows. Our model is designed to leverage longer lookback windows more effectively, which can potentially lead to even better forecasting performance. However, due to time and resource constraints, we have not conducted a comprehensive evaluation across extended lookback lengths. We plan to include this analysis in future work to further validate the robustness of our approach. We observed that the Exchange dataset is highly sensitive to the length of the lookback window, and its forecasting performance drops substantially as the window increases across all model. To ensure fairness and representativeness in the long-window comparison (Table 21), we report results on the Wind1 dataset.

Short-term Forecasting. To validate the effectiveness of our approach in short-term forecasting, we selected a representative subset of baseline models for comparison, as shown in Table 17. Under unified experimental settings, our method achieves consistently competitive performance across multiple traffic datasets. While we do not claim absolute superiority, the results indicate that our design is capable of delivering robust short-term predictions without significant degradation.

ERROR BARS. In this paper, we repeat the experiments three times. Here we report the standard deviation of our model, as well as the statistical significance test in Table 18.

Experiment Details. All experiments were conducted on four NVIDIA A800 GPUs and implemented using PyTorch.

We ran each experiment three times and report the average results. The initial learning rate was set to 10^{-3} and optimized using the Adam optimizer with MAE loss. We applied an early stopping strategy with a patience of 3 epochs. The batch size was set to 16 for smaller datasets such as ECL, Traffic, and Solar, and 32 for the others. To ensure consistency across datasets, we fixed the training epochs to 10. Model configurations, including the number of layers, hidden dimensions, and attention heads, were selected based on dataset scale and complexity to balance performance and efficiency. Detailed model and training settings are summarized in Table 11 about Table 21.

Effect of Lookback Window. To investigate how models perform under varying input lengths, we evaluate five representative methods on six datasets with a fixed prediction length of 96 and increasing lookback windows ranging from 96 to 736. As illustrated in Figure 11, the performance of each model exhibits distinct trends as the input window lengthens. Traditional models like DLinear generally benefit from longer inputs, showing steady MAE improvements on datasets such as ETTh2 and Weather. In contrast, token-heavy transformer models like PatchTST and iTransformer often degrade in performance with longer inputs, likely due to the increased difficulty in extracting relevant temporal patterns from excessive tokens. SimpleTM shows moderate stability but still suffers mild degradation on some datasets.

Notably, TimeMosaic consistently achieves the lowest MAE across all datasets and most input lengths, demonstrating superior robustness to input size variation. For example, on the ETTh2 dataset, TimeMosaic maintains low and stable MAE across all input lengths (from 0.3294 to 0.3445), while PatchTST and iTransformer show increasing errors. This suggests that our model’s adaptive granularity mechanism and segment-wise decoding enable it to effectively utilize longer contexts without overfitting or introducing noise,

Dataset	d_{model}	d_{ff}	Layers	Heads	Batch Size	Epochs	LR*	Patience
ECL	128	256	1	2	16	10	10^{-4}	3
Traffic	128	256	1	2	16	10	10^{-4}	3
Solar	128	256	1	2	16	10	10^{-4}	3
ETTh1	512	2048	2	8	32	10	10^{-4}	3
ETTh2	512	2048	2	8	32	10	10^{-4}	3
ETTM1	512	2048	2	8	32	10	10^{-4}	3
ETTM2	512	2048	2	8	32	10	10^{-4}	3
Weather	512	2048	2	8	32	10	10^{-4}	3
Exchange	512	2048	2	8	32	10	10^{-4}	3
Wind	512	2048	2	8	32	10	10^{-4}	3

Table 11: Experiment configuration of TimeMosaic in Table 21. All experiments use the Adam optimizer with a learning rate of 10^{-3} and early stopping (patience = 3).

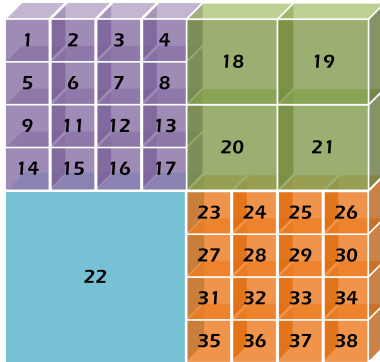


Figure 13: Overview of position embedding adopted in ours.

supporting both scalability and stability.

Experimental Settings and Fairness Considerations. To ensure a fair and reproducible comparison across models, we adopt a unified evaluation setting in Table 21, which is more rigorous than the setup used in Table 20. Specifically, Table 21 employs an extended lookback window, enabling models such as DUET and TimeFilter to better realize their potential. Furthermore, to avoid test-set-driven tuning, we strictly fix all major hyperparameters, including d_{model} , d_{ff} , the number of layers, attention heads, learning rate, training epochs, patience, and batch size. We summarize the detailed hyperparameter settings in Table 12.

Note that we excluded PathFormer from Table 21 due to its excessive GPU memory requirements when extending the lookback window, which made its evaluation computationally infeasible.

Ablation on Normalization, Position Encoding, and Budget Loss Settings. Table 19 presents a comprehensive comparison of ablation studies on the Wind1–Wind4 datasets, focusing on three key model components: normalization method, position encoding strategy, and budget loss configuration. Specifically, we compare the following variants:

- **TimeMosaic:** The standard model, using z-score normal-

ization, sinusoidal position encoding, and a default budget loss weight of 0.01.

- **RevIn:** Replaces z-score normalization with RevIN (Kim et al. 2021). We note that z-score normalization is also used for all experiments in Table 20.
- **LearnPos:** Substitutes sinusoidal encoding with learnable position embeddings. For adaptive patching, positional indices are assigned sequentially starting from each region (see visualization in Fig. 13).
- **NoPos:** Removes position encoding entirely.
- **Budget_{0.001}:** Sets budget loss weight to 0.001.
- **NoBudget:** Removes budget loss term.

All variants are evaluated on the Wind1–Wind4 datasets, using the same backbone architecture.

As shown in Table 25, we compare z-score and RevIN normalization across eight benchmark datasets and four forecasting horizons. We observe that RevIN achieves lower MSE or MAE in the majority of cases, especially on datasets such as ETTh1, Weather, and Solar-Energy. However, z-score normalization still performs competitively on datasets like ETTm1 and Traffic. These results suggest that the effectiveness of normalization methods is data-dependent, and RevIN tends to offer better robustness on datasets with complex or shifting distributions.

Analysis. Across all settings, TimeMosaic and its ablations demonstrate robust performance. Notably, switching from z-score to RevIN normalization provides a slight and consistent improvement in MSE and MAE across most datasets and horizons, indicating RevIN’s suitability for wind series with non-stationary statistics.

Replacing sinusoidal with learnable position encodings (LearnPos) yields comparable or slightly improved results, confirming the effectiveness of data-driven position embeddings when patch boundaries are not fixed. In contrast, removing positional encoding (NoPos) generally leads to marginally worse performance, highlighting the importance of explicit temporal cues, especially under adaptive patching.

Regarding budget loss, decreasing its weight from 0.01 to 0.001 (Budget_{0.001}) or removing it altogether (NoBud-

Datasets	d_model	d_ff	Layers	Heads	LR	Epochs (Patience)	Batch Size
ETT, Weather, Exchange	512	2048	2	8	0.0001	10 (3)	32
Traffic, Electricity, Solar	128	256	1	2	0.0001	10 (3)	16
Traffic (TimeFilter only)	128	256	1	2	0.0001	10 (3)	2*

Table 12: Unified hyperparameter settings used for experiments in Table 21. *Batch size is set to 2 specifically for TimeFilter on Traffic due to GPU memory constraints (59,551 MiB / 81,920 MiB).

get) results in nearly identical outcomes, suggesting that the model is relatively insensitive to this hyperparameter within the tested range.

Overall, these results validate the robustness of TimeMosaic to different normalization, positional encoding, and budget loss configurations.

H Detailed Analysis of Forecasting Results.

Table 21 presents an extensive evaluation of our proposed method TimeMosaic compared to eleven state-of-the-art baseline models across eight widely-used multivariate time series datasets (ETTm1, ETTm2, ETTh1, ETTh2, Weather, Electricity, Traffic, Solar-Energy, Wind) with four prediction horizons (96, 192, 336, and 720). Our analysis highlights TimeMosaic’s consistent superiority in forecasting performance, and we summarize key insights below.

1) Comprehensive Performance Advantage. TimeMosaic distinctly outperforms all competing methods in terms of the number of times it achieves top performance, leading in 32 cases—significantly ahead of other models such as TimeFilter (22 cases) and DUET (16 cases). This demonstrates TimeMosaic’s broad effectiveness and robustness in diverse forecasting contexts.

2) Dataset-specific Observations. On ETTm1, TimeMosaic shows a clear advantage at the longest horizon (720), achieving the best MSE/MAE and the lowest average MAE across all horizons. On ETTm2, it consistently ranks in the top two, with particularly strong long-term forecasting. On ETTh1 and ETTh2, it outperforms others in average metrics and maintains strong short-horizon accuracy. On *Weather* and *Solar-Energy*, TimeMosaic performs best or second-best in most cases, validating its generalization to nonlinear and periodic signals. On *Electricity* and *Traffic*, it remains competitive with TimeFilter, ranking second-best in MAE consistently. On *Wind*, despite LightTS’s lead, TimeMosaic still ranks second-best on average, demonstrating robust behavior on highly volatile data.

3) Horizon-wise Analysis. TimeMosaic maintains strong performance across all horizons. Its capability is especially notable at longer horizons (e.g., ETTm1 at 720 with MAE = 0.413), highlighting its effectiveness in reducing long-range error accumulation.

4) Methodological Insights. The superior performance of TimeMosaic stems from its *adaptive patch embedding* and *segment-wise prompt tuning*, which jointly address temporal heterogeneity in both input and output. Unlike fixed-patch methods (e.g., PatchTST) or simple baselines (e.g., DLinear), our design enables finer modeling where needed

and coarser abstraction elsewhere, achieving high accuracy with efficiency.

Overall, the results in Table 21 show that **TimeMosaic** sets a new state-of-the-art in long-term multivariate forecasting, demonstrating consistent, robust, and interpretable performance across diverse datasets and conditions.

I Hyperparameter Search Protocol

To ensure a fair comparison across models, we adopt a unified grid-search strategy on standard long-term forecasting benchmarks (ETTh1, ETTh2, ETTm1, ETTm2, Weather). The search space covers input sequence lengths {96, 192, 320, 512}, prediction horizons {96, 192, 336, 720}, model dimensions {16, 128, 512} with feed-forward size $4 \times d_{\text{model}}$, encoder depths {1, 3, 5}, training epochs {10, 50, 100}, and learning rates $\{10^{-5}, 10^{-4}, 10^{-3}, 10^{-2}, 0.05\}$. Other hyperparameters (batch size, number of heads, decoder layers, etc.) follow common defaults to keep the search tractable. This design yields 2160 configurations per dataset, leading to **10,800** candidate runs per model over the five datasets considered. Results are reported based on the best validation performance under this unified search space.

For fairness, all models are treated identically. When models involve auxiliary loss terms in addition to the main forecasting objective, we fix the auxiliary loss weight to 0.001, including for TimeMosaic. Model-specific hyperparameters such as the number and size of granularities in TimeMosaic, or the `topk` parameter in other architectures, are kept at their default values rather than tuned. Likewise, dropout is uniformly disabled across all methods to avoid providing implicit advantages to any single model. Finally, certain models such as DLinear do not make use of `d_model` or feed-forward dimensions; in these cases, the corresponding search dimensions are skipped.

J Comparison with TSFMs

To further evaluate the scalability and generalization ability of TimeMosaic, we conduct large-scale experiments under the same settings as Table 21, comparing against representative Time Series Foundation Models (TSFMs). Specifically, TimeMosaic is trained with an input length of 512 and an output horizon of 720 on two NVIDIA V100 GPUs, requiring approximately 40 hours of training. The forecasting segment length is set to 16, with `train_epochs`=1, batch size of 256, a single Transformer layer, and 8 attention heads. The prompt embedding dimension is 8, and the adaptive patch search space is defined as [8, 16, 32, 64].

Patch granularity	ETTh1		ETTh2		ETTm1		ETTm2		Exchange		Weather		Average	
	MSE	MAE												
[8, 16]	0.363	0.389	0.296	0.341	0.295	0.332	0.168	0.248	0.106	0.230	0.155	0.190	0.231	0.288
[4, 8, 16, 32]	0.370	0.391	0.297	0.342	0.292	0.332	0.171	0.249	0.099	0.222	0.156	0.191	0.232	0.290
[8, 16, 32]	0.359	0.387	0.307	0.346	0.300	0.339	0.169	0.248	0.105	0.230	0.154	0.190	0.231	0.289
[8, 16, 32, 64]	0.359	0.384	0.298	0.341	0.295	0.336	0.167	0.246	0.093	0.217	0.153	0.191	0.228	0.286
[8, 16, 64]	0.363	0.386	0.295	0.340	0.294	0.337	0.171	0.250	0.105	0.230	0.154	0.192	0.230	0.289
[8, 32]	0.355	0.382	0.298	0.341	0.289	0.332	0.173	0.251	0.097	0.219	0.153	0.189	0.228	0.286
[8, 32, 64]	0.369	0.390	0.306	0.345	0.303	0.336	0.166	0.245	0.108	0.231	0.155	0.191	0.235	0.289

Table 13: Performance comparison of different patch granularities across six datasets ($L = 320$, $H = 96$).

Dataset	Baseline		+APE		+APE + Prompt	
	MSE	MAE	MSE	MAE	MSE	MAE
ETTh1	0.403	0.423	0.361	0.387	0.362	0.387
ETTh2	0.324	0.374	0.297	0.342	0.300	0.342
ETTm1	0.321	0.361	0.298	0.335	0.304	0.344
ETTm2	0.181	0.270	0.172	0.251	0.164	0.247
Weather	0.155	0.204	0.160	0.196	0.144	0.189
Average	0.277	0.326	0.258	0.302	0.254	0.301

Table 14: Ablation results on five datasets with different module combinations. The length of input is 96.

We adopt the BLAST dataset (Shao et al. 2025) for training. Under this configuration, the total number of trainable parameters is 27,259,924.

BLAST (BaLAnced Sampling Time series corpus) is a large-scale dataset specifically constructed for pre-training universal time series models. It consists of 321 billion observations, mainly from CMIP6 (Eyring et al. 2016) (32.5%), ERA5 (Hersbach et al. 2020) (30.0%), Weather-Bench (Rasp et al. 2020) (25.7%), Buildings_900K (Emami, Sahu, and Graf 2023) (6.9%), and over 300 additional public datasets (Shao et al. 2025) (4.9%), covering diverse domains such as climate, meteorology, and energy. To ensure the independence of downstream evaluation, commonly used benchmark datasets (e.g., ETTh/ETTm, Weather, GlobalTemp) are deliberately excluded. In our experiments, we adopt random sampling on BLAST to generate training data, ensuring broad coverage of diverse patterns.

Table 24 reports the zero-shot forecasting results of TimeMosaic across six datasets. The results demonstrate that, when trained on large-scale data, TimeMosaic achieves performance comparable to state-of-the-art TSFMs, highlighting the structural advantages of our design. In particular, the adaptive patch embedding and segment-wise decoding modules enable effective utilization of long historical contexts and robust adaptation to diverse prediction horizons, which is crucial for foundation-model-level generalization.

As shown in Table 16, TimeMosaic maintains a balanced trade-off between model scale and inference efficiency. Its parameter count (27M) is larger than extremely compact baselines such as Moirai-Small (14M), yet smaller than medium- and large-scale TSFMs (e.g., Chronos-Small

at 48M, Chronos-Base at 205M, and TimeMoe-200M at 453M). More importantly, TimeMosaic achieves the fastest inference speed among all compared models (0.068s), substantially outperforming both small baselines (e.g., Moirai-Small at 0.350s, Chronos-Small at 0.256s) and heavyweight TSFMs. These results confirm that TimeMosaic achieves a highly favorable balance between scalability and efficiency, making it well-suited for both research and practical deployment.

K Limitations and Future work

While TimeMosaic achieves state-of-the-art forecasting performance, several limitations provide opportunities for future research. Firstly, TimeMosaic currently utilizes a moderate parameter scale, which restricts its capability to capture complex long-range dependencies. Future research could scale TimeMosaic into a foundational model via large-scale pretraining, potentially enhancing its temporal representation and cross-domain generalization. Secondly, TimeMosaic employs fixed prediction horizons, limiting its adaptability. Future work should develop dynamic, adaptive prediction horizons responsive to real-time data characteristics, improving practicality in streaming scenarios. Lastly, integrating continuous learning capabilities could help TimeMosaic effectively handle temporal non-stationarities, maintaining long-term forecasting accuracy without frequent retraining. Addressing these aspects will significantly enhance TimeMosaic’s robustness and practical applicability.

L Why called TimeMosaic?

The name ‘TimeMosaic’ reflects our core idea of decomposing time series into a flexible arrangement of patches of variable length, much like assembling a mosaic from tiles of different shapes and sizes. By adaptively segmenting the sequence based on local information density, our model constructs a holistic and coherent temporal representation, where each patch plays a distinct but integrated role, analogous to mosaic fragments collectively forming a complete picture. This flexible composition enables the model to efficiently capture both fine-grained and coarse-grained patterns, addressing the inherent heterogeneity of real-world time series.

Dataset	Model	MSE	MAE	Total Parameter	Inference Time (s)	GPU Memory Footprint (MB)	Peak Mem (MB)
ETTh1	TimeMosaic	0.413	0.428	365,825	0.059504	21.78	161.29
	TimeFilter	0.425	0.438	1,830,640	0.014385	81.95	240.01
	SimpleTM	0.429	0.443	9,893,368	0.017082	94.06	872.34
	iTransformer	0.437	0.450	3,588,432	0.002159	45.95	53.66
	PatchTST	0.423	0.437	2,953,424	0.002301	43.54	155.70
ETTh2	TimeMosaic	0.370	0.397	2,367,329	0.010097	38.73	121.91
	TimeFilter	0.368	0.411	176,460	0.006502	26.61	175.04
	SimpleTM	0.381	0.413	14,216	0.003503	18.30	146.40
	iTransformer	0.385	0.415	14,160	0.002070	18.29	19.75
	PatchTST	0.384	0.413	232,064	0.005510	20.29	99.58
ETTm1	TimeMosaic	0.356	0.374	227,169	0.033050	20.28	155.07
	TimeFilter	0.362	0.384	111,444	0.005413	25.37	83.53
	SimpleTM	0.362	0.387	3,490,184	0.005095	44.81	822.48
	iTransformer	0.370	0.394	12,112	0.003450	18.01	19.37
	PatchTST	0.362	0.389	139,488	0.003512	19.31	40.52
ETTm2	TimeMosaic	0.269	0.318	365,825	0.031740	21.78	161.29
	TimeFilter	0.272	0.329	118,076	0.010274	25.44	83.88
	SimpleTM	0.273	0.328	1,076,328	0.079104	26.40	76.93
	iTransformer	0.287	0.340	17,232	0.003550	18.71	20.57
	PatchTST	0.272	0.333	347,968	0.002239	21.54	109.19
Weather	TimeMosaic	0.240	0.267	372,413	0.055469	26.30	342.41
	TimeFilter	0.237	0.278	179,148	0.032229	35.48	1363.94
	SimpleTM	0.238	0.276	17,400	0.008303	22.97	26.05
	iTransformer	0.247	0.284	1,100,624	0.006658	31.22	36.37
	PatchTST	0.243	0.279	347,968	0.002607	25.80	288.75

Table 15: Comparison of model performance and resource utilization across different datasets. Metrics include Mean Squared Error (MSE), Mean Absolute Error (MAE), total parameter count, inference time (seconds), GPU memory footprint (MB), and peak memory usage (MB), the predicted length is fixed 336.

Table 16: Comparison of model size and inference efficiency. TimeMosaic maintains a moderate parameter scale and inference latency compared to existing TSFMs.

Model	Params	Inference Time (s)
TimeMoe-50M	113M	5.725
TimeMoe-200M	453M	10.813
Moirai-Small	14M	0.350
Moirai-Base	91M	0.483
Moirai-Large	311M	0.894
Chronos-Small	48M	0.256
Chronos-Base	205M	0.409
TimeMosaic (Ours)	27M	0.068

Models	TimeMosaic (Ours)		SimpleTM (2025)		xPatch (2025)		DLinear (2023)		PatchTST (2023)	
	MSE	MAE	MSE	MAE	MSE	MAE	MSE	MAE	MSE	MAE
PEMS03	0.075	0.185	0.093	0.207	0.085	<u>0.195</u>	0.105	0.221	<u>0.092</u>	0.208
PEMS04	0.094	<u>0.208</u>	<u>0.094</u>	0.207	0.103	0.213	0.115	0.228	0.110	0.226
PEMS07	<u>0.075</u>	0.188	0.074	0.187	0.078	0.187	0.100	0.216	0.086	0.203
PEMS08	0.090	<u>0.207</u>	<u>0.096</u>	0.206	0.097	0.204	0.112	0.223	0.104	0.222

Table 17: Averaged forecasting results under unified experimental settings. For **short-term** forecasting tasks, we use a fixed lookback window of $L = 96$. Short-term forecasting uses a single-step prediction length $T = 12$. The best model is in **boldface**, and the second best is underlined.

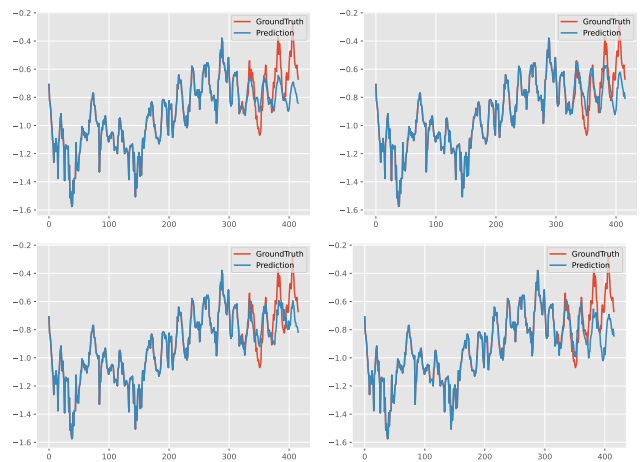


Figure 14: Prediction cases from ETTh1 by different models (TimeMosaic, SimpleTM, PatchTST, iTransformer) under input-320-predict-96 settings.

Dataset	TimeMosaic (Ours)		SimpleTM (ICLR'2025)		Confidence Interval
	MSE	MAE	MSE	MAE	
Weather	0.251 ± 0.004	0.267 ± 0.003	0.258 ± 0.005	0.282 ± 0.004	99%
Solar	0.240 ± 0.005	0.270 ± 0.004	0.315 ± 0.006	0.333 ± 0.005	99%
Electricity	0.187 ± 0.006	0.279 ± 0.004	0.248 ± 0.007	0.284 ± 0.006	99%
Traffic	0.458 ± 0.008	0.283 ± 0.005	0.545 ± 0.009	0.347 ± 0.007	99%
ETTh1	0.425 ± 0.006	0.424 ± 0.004	0.442 ± 0.005	0.436 ± 0.004	99%
ETTh2	0.363 ± 0.005	0.388 ± 0.006	0.424 ± 0.006	0.413 ± 0.005	99%
ETTm1	0.381 ± 0.004	0.381 ± 0.004	0.391 ± 0.005	0.403 ± 0.004	99%
ETTm2	0.273 ± 0.003	0.314 ± 0.003	0.283 ± 0.004	0.325 ± 0.004	99%
Exchange	0.348 ± 0.005	0.403 ± 0.004	0.356 ± 0.005	0.411 ± 0.005	99%

Table 18: Standard deviation and statistical tests for our TimeMosaic method and second-best method (SimpleTM) on ETT, Weather, Solar, Electricity and Traffic datasets.

Methods	TimeMosaic		Revin		LearnPos		NoPos		<i>Budget</i> _{0.001}		NoBudget		
Metric	MSE	MAE	MSE	MAE	MSE	MAE	MSE	MAE	MSE	MAE	MSE	MAE	
Wind1	96	<u>0.765</u>	0.668	0.760	0.661	0.769	0.668	0.768	0.668	<u>0.765</u>	<u>0.667</u>	<u>0.765</u>	<u>0.667</u>
	192	<u>0.819</u>	<u>0.701</u>	0.813	0.693	0.822	0.701	0.822	<u>0.701</u>	<u>0.820</u>	<u>0.701</u>	0.822	0.702
	336	<u>0.860</u>	<u>0.722</u>	0.852	0.715	0.860	<u>0.722</u>	<u>0.859</u>	<u>0.722</u>	0.861	0.724	0.862	0.723
	720	<u>0.884</u>	<u>0.738</u>	0.880	0.733	<u>0.883</u>	<u>0.738</u>	<u>0.883</u>	<u>0.738</u>	0.886	0.739	0.885	0.739
	Avg	<u>0.832</u>	<u>0.707</u>	0.826	0.700	0.834	<u>0.707</u>	0.833	<u>0.707</u>	0.833	0.708	0.833	0.708
Wind2	96	0.747	0.655	0.736	0.646	0.747	0.654	0.747	0.654	<u>0.745</u>	0.654	<u>0.745</u>	<u>0.653</u>
	192	<u>0.811</u>	<u>0.693</u>	0.805	0.687	0.813	0.694	0.814	0.694	0.812	0.694	0.816	0.695
	336	0.845	0.713	0.839	0.706	0.846	0.713	<u>0.844</u>	<u>0.712</u>	0.846	0.713	0.847	0.713
	720	<u>0.878</u>	<u>0.733</u>	0.874	0.728	0.883	0.735	0.880	0.734	<u>0.878</u>	<u>0.733</u>	0.880	0.734
	Avg	<u>0.820</u>	<u>0.698</u>	0.813	0.692	0.822	0.699	0.821	<u>0.698</u>	<u>0.820</u>	<u>0.698</u>	0.822	0.699
Wind3	96	<u>0.754</u>	<u>0.650</u>	0.745	0.643	0.756	0.652	0.757	0.652	<u>0.754</u>	<u>0.650</u>	0.755	<u>0.650</u>
	192	<u>0.808</u>	<u>0.686</u>	0.804	0.682	0.815	0.689	0.813	0.688	0.810	0.687	0.814	0.688
	336	0.843	<u>0.708</u>	0.843	0.705	0.843	0.709	<u>0.845</u>	0.709	<u>0.845</u>	0.709	0.850	0.710
	720	<u>0.883</u>	<u>0.727</u>	0.882	0.725	0.884	0.728	0.885	0.729	0.886	0.729	0.889	0.729
	Avg	<u>0.822</u>	<u>0.693</u>	0.819	0.689	0.825	0.694	0.825	0.695	0.824	<u>0.693</u>	0.827	0.694
Wind4	96	0.820	0.687	0.809	0.679	0.818	<u>0.687</u>	0.819	0.688	0.820	0.688	0.820	<u>0.687</u>
	192	<u>0.871</u>	<u>0.723</u>	0.866	0.716	0.873	<u>0.723</u>	0.873	<u>0.723</u>	0.874	0.724	0.876	0.725
	336	<u>0.898</u>	<u>0.738</u>	0.891	0.730	0.899	<u>0.738</u>	<u>0.898</u>	<u>0.738</u>	<u>0.898</u>	<u>0.738</u>	0.900	0.739
	720	<u>0.937</u>	0.758	0.931	0.750	<u>0.937</u>	0.758	<u>0.937</u>	<u>0.757</u>	0.939	0.759	0.941	0.759
	Avg	<u>0.881</u>	<u>0.726</u>	0.874	0.718	0.882	0.727	0.882	0.727	0.883	0.727	0.884	0.727

Table 19: Full results on Wind datasets under various ablation settings. We compare the original TimeMosaic with: (i) RevIN normalization, (ii) learnable and removed positional encoding, (iii) reduced or removed budget loss. All models are evaluated without any downstream fine-tuning. Results are reported as MSE and MAE (lower is better). The input length is 96. For details on position encoding visualization, see Fig. 13.

Models		TimeMosaic	SimpleTM		TimeFilter		xPatch		PatchMLP		DUET		PathFormer		iTransformer		TimeMxier		PatchTST		DLinear		FreTS	
		Ours	(2025)		(2025)		(2025)		(2025)		(2025b)		(2024)		(2024a)		(2024)		(2023)		(2023)		(2023)	
Metric		MSE MAE	MSE MAE	MSE MAE	MSE MAE	MSE MAE	MSE MAE	MSE MAE	MSE MAE	MSE MAE	MSE MAE	MSE MAE	MSE MAE	MSE MAE	MSE MAE	MSE MAE	MSE MAE	MSE MAE	MSE MAE	MSE MAE	MSE MAE	MSE MAE	MSE MAE	MSE MAE
ETTm1	96	0.308 0.338	0.323 0.364	0.317 0.359	0.332 0.369	0.329 0.367	0.359 0.375	<u>0.315</u> <u>0.345</u>	0.330 0.365	0.327 0.362	0.320 0.361	0.345 0.372	0.340 0.375											
	192	<u>0.364</u> 0.368	0.371 0.389	0.381 0.393	0.371 0.387	0.377 0.394	0.394 0.393	0.375 <u>0.372</u>	0.388 0.399	0.358 0.380	<u>0.364</u> 0.382	0.389 0.396	0.392 0.406											
	336	<u>0.394</u> 0.390	0.411 0.413	0.402 0.409	0.399 0.407	0.411 0.413	0.426 0.413	0.405 0.393	0.417 0.416	0.385 0.400	0.402 0.406	0.419 0.417	0.428 0.429											
	720	0.460 0.428	0.460 0.445	0.481 0.468	0.463 0.443	0.485 0.454	0.486 0.448	0.471 0.430	0.499 0.465	0.455 0.443	<u>0.461</u> <u>0.442</u>	0.476 0.452	0.495 0.472											
	Avg.	0.381 0.381	0.391 0.403	0.395 0.407	0.391 0.402	0.401 0.407	0.416 0.407	0.392 <u>0.385</u>	0.409 0.411	0.381 0.396	<u>0.387</u> 0.398	0.407 0.409	0.414 0.421											
ETTm2	96	<u>0.170</u> <u>0.248</u>	0.178 0.256	0.174 0.259	0.177 0.262	0.178 0.262	0.182 0.265	0.166 0.247	0.182 0.263	0.176 0.257	0.178 0.260	0.194 0.293	0.193 0.284											
	192	<u>0.236</u> 0.291	0.242 0.300	0.241 0.304	0.244 0.306	0.244 0.307	0.246 0.305	0.232 <u>0.292</u>	0.257 0.315	0.246 0.306	0.240 0.299	0.291 0.367	0.272 0.348											
	336	<u>0.295</u> <u>0.331</u>	0.309 0.344	0.305 0.344	0.304 0.342	0.307 0.343	0.307 0.343	0.290 <u>0.329</u>	0.314 0.350	0.296 0.339	0.299 0.338	0.373 0.421	0.376 0.409											
	720	<u>0.392</u> 0.386	0.401 0.399	0.410 0.407	0.404 0.399	0.420 0.413	0.408 0.399	0.386 <u>0.387</u>	0.418 0.409	0.396 0.396	0.399 0.396	0.541 0.518	0.507 0.494											
	Avg.	<u>0.273</u> 0.314	0.283 <u>0.325</u>	0.282 0.329	0.283 0.327	0.287 0.331	0.286 0.328	0.269 0.314	0.293 0.334	0.279 0.325	0.279 0.323	0.350 0.400	0.337 0.384											
ETTth1	96	0.369 0.389	0.379 <u>0.396</u>	0.396 0.403	0.383 0.401	0.392 0.405	0.391 0.403	0.391 0.392	0.382 0.400	<u>0.374</u> 0.397	0.377 0.393	0.396 0.411	0.397 0.409											
	192	0.416 0.415	0.432 0.425	0.467 0.446	0.431 0.427	0.442 0.434	0.437 0.428	0.442 0.419	0.443 0.433	0.432 0.429	<u>0.426</u> 0.422	0.447 0.443	0.455 0.448											
	336	0.454 0.435	0.476 0.448	0.486 0.456	0.483 0.455	0.483 0.455	0.479 0.451	0.487 0.439	0.480 0.452	0.481 0.451	<u>0.464</u> <u>0.443</u>	0.496 0.473	0.507 0.478											
	720	0.461 0.458	<u>0.481</u> 0.473	0.503 0.481	0.486 0.474	0.502 0.484	0.482 0.477	0.494 <u>0.463</u>	0.493 0.481	0.493 0.477	0.461 0.465	0.510 0.508	0.553 0.530											
	Avg.	0.425 0.424	0.442 0.436	0.463 0.447	0.446 0.439	0.455 0.445	0.447 0.440	0.454 0.428	0.450 0.442	0.445 0.439	<u>0.432</u> <u>0.431</u>	0.462 0.459	0.478 0.466											
ETTth2	96	<u>0.286</u> 0.332	0.308 0.356	0.295 0.346	0.291 0.343	0.309 0.359	0.290 0.340	0.284 <u>0.333</u>	0.305 0.352	0.290 0.341	0.292 0.343	0.347 0.401	0.369 0.411											
	192	0.362 0.380	0.383 0.404	0.412 0.423	0.372 0.392	0.405 0.419	0.377 0.393	0.366 0.387	0.378 0.398	<u>0.371</u> <u>0.391</u>	0.372 0.396	0.463 0.469	0.457 0.466											
	336	0.409 0.416	0.422 0.436	0.456 0.449	0.423 0.433	0.432 0.441	0.419 0.429	<u>0.410</u> <u>0.421</u>	0.420 0.427	0.423 0.432	0.414 0.426	0.573 0.533	0.547 0.519											
	720	0.396 0.422	0.442 0.454	0.474 0.469	0.430 0.451	0.460 0.446	0.428 0.443	0.428 0.445	0.441 0.451	0.439 0.450	<u>0.425</u> <u>0.441</u>	0.839 0.661	0.713 0.606											
	Avg.	0.363 0.388	0.424 0.413	0.389 0.422	0.409 0.405	0.402 0.416	0.379 0.400	<u>0.372</u> <u>0.397</u>	0.386 0.407	0.381 0.404	0.376 0.402	0.556 0.516	0.522 0.501											
Weather	96	0.165 <u>0.198</u>	0.175 0.219	<u>0.156</u> <u>0.203</u>	0.178 0.221	0.165 0.211	0.192 0.233	0.155 0.197	0.175 0.214	0.163 0.210	0.183 0.222	0.196 0.256	0.185 0.240											
	192	0.215 <u>0.243</u>	0.217 0.257	<u>0.208</u> 0.253	0.231 0.263	0.212 0.252	0.236 0.269	0.203 0.241	0.227 0.261	0.208 0.251	0.226 0.258	0.236 0.295	0.223 0.273											
	336	0.272 0.286	0.282 0.302	0.263 0.293	0.283 0.300	0.283 0.305	0.287 0.304	<u>0.265</u> <u>0.287</u>	0.285 0.301	0.268 0.295	0.286 0.300	0.283 0.333	0.277 0.320											
	720	0.353 <u>0.340</u>	0.357 0.351	0.340 0.342	0.360 0.350	0.357 0.352	0.359 0.350	<u>0.344</u> 0.337	0.360 0.350	0.346 0.348	0.360 0.352	0.346 0.383	0.345 0.375											
	Avg.	<u>0.251</u> <u>0.267</u>	0.258 0.282	0.242 0.273	0.264 0.284	0.254 0.289	0.269 0.304	0.242 0.266	0.346 0.276	0.309 0.360	0.264 0.283	0.265 0.317	0.256 0.302											
Electricity	96	0.160 0.258	0.176 0.258	0.142 0.241	0.191 0.277	0.156 0.257	0.204 0.292	0.199 0.269	0.158 0.248	<u>0.156</u> <u>0.248</u>	0.180 0.269	0.200 0.287	0.187 0.274											
	192	0.174 0.269	0.184 0.267	0.159 0.256	0.193 0.278	0.174 0.270	0.205 0.296	0.203 0.276	<u>0.170</u> <u>0.259</u>	<u>0.170</u> 0.261	0.188 0.277	0.200 0.290	0.190 0.278											
	336	0.189 0.283	0.204 0.289	0.173 0.271	0.206 0.291	0.199 0.297	0.221 0.310	0.210 0.302	0.187 <u>0.276</u>	<u>0.186</u> <u>0.276</u>	0.204 0.294	0.212 0.305	0.206 0.295											
	720	<u>0.225</u> <u>0.304</u>	0.244 0.321	0.206 0.297	0.244 0.321	0.242 0.331	0.264 0.344	0.245 0.326	0.280 0.363	0.228 0.312	0.247 0.329	0.248 0.338	0.244 0.330											
	Avg.	0.187 <u>0.279</u>	0.248 0.284	0.170 0.192	0.209 0.292	0.224 0.289	0.216 0.311	0.214 0.293	0.225 0.310	<u>0.185</u> 0.294	0.205 0.292	0.215 0.305	0.207 0.294											
Traffic	96	<u>0.424</u> 0.269	0.531 0.337	0.431 0.297	0.521 0.346	0.466 0.322	0.649 0.402	0.551 0.326	0.421 0.289	0.480 0.298	0.463 0.302	0.652 0.400	0.529 0.341											
	192	0.448 0.279	0.530 0.342	<u>0.447</u> 0.299	0.506 0.330	0.475 0.325	0.602 0.381	0.553 0.334	0.442 0.296	0.492 0.305	0.470 0.306	0.601 0.374	0.531 0.339											
	336	0.464 0.284	0.542 0.347	<u>0.462</u> 0.307	0.511 0.327	0.496 0.338	0.611 0.383	0.587 0.332	0.459 0.305	0.504 <u>0.304</u>	0.487 0.313	0.608 0.377	0.552 0.347											
	720	<u>0.495</u> 0.301	0.576 0.360	0.502 0.331	0.540 0.338	0.542 0.362	0.651 0.402	0.631 0.378	0.491 0.323	0.521 <u>0.320</u>	0.522 0.334	0.648 0.398	0.599 0.367											
	Avg.	<u>0.458</u> 0.283	0.545 0.347	0.461 0.309	0.520 0.335	0.495 0.337	0.628 0.392	0.581 0.343	0.453 0.303	0.499 <u>0.291</u>	0.486 0.314	0.627 0.387	0.553 0.349											
Solar-Energy	96	<u>0.209</u> <u>0.248</u>	0.252 0.299	0.222 0.253	0.216 0.259	0.218 0.245	0.300 0.328	0.208 0.231	0.301 0.333	0.242 0.342	0.217 0.258	0.285 0.372	0.233 0.291											
	192	0.238 0.272	0.306 0.332	0.256 0.265	<u>0.244</u> 0.276	0.258 0.288	0.338 0.350	0.278 <u>0.268</u>	0.339 0.347	0.285 0.380	0.247 0.280	0.316 0.393	0.256 0.308											
	336	0.255 <u>0.277</u>	0.372 0.360	0.254 0.283	0.262 0.286	0.274 0.290	0.377 0.362	0.259 0.261	0.376 0.361	0.282 0.326	0.269 0.293	0.350 0.412	0.268 0.311											
	720	0.257 <u>0.284</u>	0.331 0.339	<u>0.258</u> 0.280	0.261 0.284	0.269 0.296	0.381 0.359	0.275 0.271	0.374 0.357	0.357 0.427	0.267 0.292	0.353 0.410	0.266 0.305											
	Avg.	0.240 <u>0.270</u>	0.315 0.333	0.248 <u>0.270</u>	0.248 0.276	0.255 0.280	0.349 0.350	0.255 0.258	0.378 0.350	0.292 0.381	0.250 0.281	0.326 0.397	0.256 0.304											
Exchange	96	<u>0.082</u> 0.200	0.088 0.206	0.096 0.215	0.089 0.208	0.093 0.213	<u>0.082</u> <u>0.199</u>	0.087 0.207	0.105 0.228	0.084 0.203	0.081 0.197	0.094 0.227	0.104 0.236											
	192	0.169 0.294	0.182 0.303	0.178 0.310	0.183 0.304	0.185 0.307	<u>0.174</u> <u>0.295</u>	0.183 0.304	0.181 0.304	0.285 0.380	0.176 0.298	0.181 0.320	0.186 0.322											
	336	<u>0.328</u> 0.414	0.321 0.411	0.362 0.435	0.338 0.422	0.339 0.423	<u>0.326</u> <u>0.413</u>	0.368 0.442	0.361 0.437	0.337 0.421	0.339 0.421	0.344 0.450	0.479 0.533											
	720	<u>0.812</u> 0.680	0.843 0.691	0.829 <u>0.682</u>	0.876 0.707	0.880 0.706	0.843 0.692	0.863 0.689	0.817 0.686	0.832 0.686	0.845 0.692	0.796 0.683	1.036 0.770											
	Avg.	0.348 0.403	0.356 0.411	0.366 0.411	0.372 0.410	0.374 0.412	0.356 0.400	0.375 0.411	0.366 0.414	0.385 0.423	0.359 0.401	<u>0.354</u> 0.420	0.451 0.465											
1 st Count		42	3	14	0	0	0	18	5	3	3	1	0											

Table 20: Full results for long-term forecasting consider prediction horizons H within $\{96, 192, 336, 512\}$. For all baselines, we adhere to the setting of the iTransformer with an input sequence length of 96. The term ‘Avg.’ represents the average results across the four prediction lengths. The best and second best outcomes are highlighted in **best** and **second**, respectively. The notation 1st Count” denotes the frequency of each method achieving the top results.

Models	TimeMosaic		SimpleTM		TimeFilter		xPatch		PatchMLP		DUET		LightTS		iTransformer		TimeMxier		PatchTST		DLinear		FreTS		
	Ours		(2025)		(2025)		(2025)		(2025)		(2025b)		(2024)		(2024a)		(2024)		(2023)		(2023)		(2023)		
Metric	MSE	MAE	MSE	MAE	MSE	MAE	MSE	MAE	MSE	MAE	MSE	MAE	MSE	MAE	MSE	MAE	MSE	MAE	MSE	MAE	MSE	MAE	MSE	MAE	
ETTm1	96	0.304	<u>0.344</u>	0.286	0.338	0.355	0.373	<u>0.293</u>	0.347	0.305	0.357	0.305	0.348	0.313	0.363	0.327	0.371	0.307	0.352	0.321	0.361	0.299	<u>0.344</u>	0.308	0.353
	192	0.339	0.364	0.326	0.364	0.376	0.396	<u>0.332</u>	0.371	0.351	0.384	0.336	<u>0.365</u>	0.350	0.387	0.357	0.388	<u>0.332</u>	0.373	0.342	0.385	0.337	0.370	0.346	0.377
	336	0.375	0.385	<u>0.364</u>	<u>0.388</u>	0.401	0.413	<u>0.364</u>	0.395	0.387	0.403	0.374	<u>0.388</u>	0.399	0.418	0.393	0.412	0.362	0.390	0.386	0.410	0.369	0.385	0.382	0.399
	720	0.422	0.413	0.424	0.426	0.465	0.449	0.428	0.432	0.454	0.441	0.425	<u>0.417</u>	0.489	0.479	0.467	0.452	0.422	0.426	0.439	0.441	<u>0.424</u>	0.419	0.440	0.433
	Avg.	0.360	0.377	0.350	<u>0.379</u>	0.399	0.408	<u>0.354</u>	0.386	0.374	0.396	0.360	0.380	0.388	0.412	0.386	0.406	0.356	0.385	0.372	0.399	0.357	0.380	0.369	0.391
ETTm2	96	0.164	0.247	0.174	0.257	0.174	0.261	0.168	0.259	0.179	0.265	<u>0.165</u>	<u>0.255</u>	0.187	0.286	0.187	0.271	0.169	0.258	0.181	0.270	0.172	0.270	0.175	0.263
	192	<u>0.226</u>	0.291	0.233	<u>0.297</u>	0.229	0.298	<u>0.226</u>	0.299	0.232	0.301	0.220	0.291	0.311	0.384	0.251	0.314	0.240	0.308	0.241	0.311	0.239	0.322	0.248	0.314
	336	<u>0.279</u>	0.324	0.279	0.330	0.312	0.351	0.281	0.337	0.285	0.334	0.272	<u>0.325</u>	0.399	0.418	0.319	0.355	0.282	0.334	0.303	0.348	0.305	0.367	0.321	0.364
	720	0.353	0.376	<u>0.367</u>	0.387	0.396	0.408	0.372	0.391	0.380	0.394	0.369	<u>0.384</u>	0.489	0.479	0.413	0.412	0.369	0.391	0.385	0.399	0.412	0.432	0.393	0.414
	Avg.	0.256	0.310	0.263	0.318	0.278	0.330	0.262	0.322	0.269	0.324	<u>0.257</u>	<u>0.314</u>	0.347	0.392	0.293	0.338	0.265	0.323	0.278	0.332	0.282	0.348	0.284	0.339
ETTth	96	0.362	0.387	0.390	0.410	0.460	0.457	0.380	0.403	0.411	0.426	<u>0.372</u>	<u>0.397</u>	0.432	0.443	0.403	0.417	0.376	0.398	0.403	0.423	0.377	0.400	0.400	0.419
	192	0.400	0.411	0.422	0.428	0.439	0.443	0.425	0.430	0.443	0.445	<u>0.410</u>	<u>0.420</u>	0.474	0.472	0.443	0.444	0.412	<u>0.420</u>	0.479	0.478	<u>0.410</u>	<u>0.420</u>	0.436	0.441
	336	<u>0.436</u>	<u>0.435</u>	0.440	0.440	0.474	0.463	0.444	0.439	0.468	0.461	0.430	0.433	0.515	0.501	0.470	0.464	0.445	0.446	0.490	0.481	0.452	0.458	0.471	0.466
	720	<u>0.451</u>	0.460	0.459	0.475	0.670	0.564	0.534	0.509	0.525	0.508	0.445	<u>0.466</u>	0.592	0.567	0.632	0.573	0.488	0.489	0.641	0.559	0.477	0.497	0.537	0.532
	Avg.	0.412	0.423	0.428	0.438	0.511	0.482	0.446	0.445	0.462	0.460	<u>0.414</u>	<u>0.429</u>	0.503	0.496	0.487	0.475	0.430	0.438	0.503	0.485	0.429	0.444	0.461	0.465
ETTth2	96	0.300	<u>0.342</u>	0.298	0.349	0.367	0.389	<u>0.280</u>	0.343	0.311	0.371	0.273	0.337	0.324	0.383	0.323	0.369	0.285	0.346	0.324	0.374	0.305	0.368	0.321	0.380
	192	0.354	0.387	0.379	0.396	0.372	0.404	<u>0.345</u>	<u>0.386</u>	0.381	0.413	0.335	0.379	0.438	0.455	0.421	0.422	0.358	0.391	0.378	0.416	0.407	0.435	0.396	0.429
	336	<u>0.378</u>	0.403	0.400	0.420	0.402	0.426	0.382	0.415	0.401	0.427	0.362	0.403	0.496	0.490	0.440	0.441	0.380	<u>0.409</u>	0.405	0.432	0.493	0.490	0.497	0.496
	720	0.421	<u>0.439</u>	0.432	0.451	0.465	0.464	<u>0.408</u>	0.443	0.426	0.451	0.406	0.437	1.151	0.749	0.459	0.466	0.410	0.439	0.484	0.484	0.762	0.620	0.766	0.628
	Avg.	0.363	<u>0.393</u>	0.377	0.404	0.402	0.421	<u>0.354</u>	0.397	0.380	0.416	0.344	0.389	0.602	0.519	0.411	0.425	0.358	0.396	0.398	0.427	0.492	0.478	0.495	0.483
Weather	96	0.144	0.189	<u>0.148</u>	<u>0.197</u>	0.156	0.209	<u>0.148</u>	<u>0.196</u>	0.153	0.206	0.176	0.227	0.152	0.212	0.160	0.209	0.150	0.199	0.155	0.204	0.177	0.242	0.156	0.213
	192	0.197	0.232	0.195	0.244	0.195	0.246	0.190	<u>0.238</u>	0.197	0.245	0.218	0.261	0.197	0.255	0.207	0.251	<u>0.193</u>	0.244	0.201	0.249	0.217	0.276	0.197	0.253
	336	0.245	0.276	0.249	0.287	0.251	0.286	0.241	<u>0.280</u>	0.247	0.282	0.265	0.294	0.249	0.299	0.256	0.289	<u>0.244</u>	0.283	0.255	0.289	0.262	0.312	0.246	0.293
	720	0.327	0.327	0.329	0.339	0.322	0.339	0.318	<u>0.333</u>	0.324	0.334	0.332	0.339	0.323	0.357	0.325	0.338	<u>0.319</u>	0.336	0.333	0.340	0.326	0.367	<u>0.319</u>	0.347
	Avg.	0.231	0.256	0.230	0.267	0.231	0.270	0.224	<u>0.262</u>	0.230	0.267	0.248	0.280	0.230	0.281	0.237	0.272	<u>0.227</u>	0.266	0.236	0.271	0.246	0.299	0.230	0.277
Electricity	96	<u>0.140</u>	<u>0.236</u>	0.146	0.245	0.137	0.233	0.143	0.241	0.165	0.271	0.152	0.257	0.171	0.285	0.145	0.244	0.141	0.238	0.142	0.245	0.143	0.242	0.144	0.245
	192	<u>0.156</u>	<u>0.250</u>	0.164	0.262	0.153	0.246	0.157	0.252	0.183	0.288	0.169	0.273	0.192	0.305	0.165	0.263	0.158	0.254	0.159	0.259	0.157	0.255	<u>0.156</u>	0.253
	336	0.173	0.267	0.183	0.281	0.169	0.263	<u>0.172</u>	<u>0.266</u>	0.201	0.304	0.188	0.291	0.214	0.324	0.184	0.282	0.175	0.270	0.176	0.276	<u>0.172</u>	0.272	0.173	0.272
	720	0.212	0.298	0.228	0.319	<u>0.208</u>	0.296	<u>0.209</u>	<u>0.297</u>	0.250	0.343	0.231	0.326	0.251	0.349	0.227	0.317	0.217	0.307	0.215	0.308	0.207	0.305	0.210	0.308
	Avg.	<u>0.170</u>	<u>0.263</u>	0.180	0.277	0.167	0.260	<u>0.170</u>	0.264	0.200	0.302	0.185	0.287	0.207	0.316	0.180	0.277	0.173	0.267	0.173	0.272	<u>0.170</u>	0.269	0.171	0.270
Traffic	96	0.409	0.274	0.429	0.313	0.397	0.274	0.413	0.297	0.486	0.361	0.426	0.309	0.493	0.367	0.422	0.310	0.421	0.297	<u>0.403</u>	0.285	0.422	<u>0.296</u>	0.417	0.301
	192	0.424	<u>0.281</u>	0.454	0.328	0.411	0.278	0.425	0.298	0.515	0.378	0.448	0.323	0.511	0.373	0.449	0.327	0.441	0.311	<u>0.419</u>	0.292	0.435	0.302	0.447	0.299
	336	0.435	<u>0.287</u>	0.474	0.341	0.423	0.284	0.430	0.297	0.533	0.386	0.468	0.334	0.521	0.378	0.469	0.339	<u>0.425</u>	0.317	0.432	0.298	0.447	0.308	0.468	0.311
	720	0.464	<u>0.302</u>	0.514	0.363	0.449	0.300	<u>0.450</u>	0.306	0.564	0.401	0.505	0.355	0.504	0.360	0.512	0.364	0.489	0.340	0.459	0.313	0.476	0.327	0.512	0.340
	Avg.	0.433	<u>0.287</u>	0.468	0.336	0.420	0.284	0.430	0.300	0.525	0.382	0.462	0.330	0.507	0.370	0.463	0.335	0.444	0.316	<u>0.428</u>	0.297	0.445	0.308	0.461	0.313
Solar-Energy	96	0.200	0.226	0.239	0.285	0.182	<u>0.240</u>	<u>0.186</u>	<u>0.240</u>	0.211	0.280	0.230	0.267	0.196	0.267	0.198	0.253	0.199	0.257	0.195	0.249	0.223	0.293	0.190	0.248
	192	0.225	0.240	0.264	0.305	0.199	0.255	0.199	<u>0.254</u>	0.245	0.285	0.260	0.284	0.211	0.280	0.222	0.276	0.221	0.274	<u>0.208</u>	0.257	0.251	0.311	0.209	0.266
	336	0.238	0.245	0.289	0.325	<u>0.207</u>	<u>0.262</u>	0.205	<u>0.257</u>	0.271	0.302	0.285	0.301	0.229	0.299	0.251	0.293	0.230	0.284	0.220	0.269	0.272	0.327	0.222	0.274
	720	0.241	0.251	0.295	0.339	<u>0.213</u>	0.264	0.209	<u>0.261</u>	0.272	0.303	0.285	0.303	0.232	0.304	0.256	0.299	0.224	0.290	0.220	0.272	0.274	0.320	0.228	0.278
	Avg.	0.226	0.241	0.272	0.314	0.200	0.255	0.200	<u>0.253</u>																

Models		TimeMosaic Ours		SimpleTM (2025)		TimeFilter (2025)		DUET (2025b)		iTransformer (2024a)		TimeMixer (2024)		PatchTST (2023)		DLinear (2023)	
Metric		MSE	MAE	MSE	MAE	MSE	MAE	MSE	MAE	MSE	MAE	MSE	MAE	MSE	MAE	MSE	MAE
ETTh1	96	<u>0.282</u>	0.328	0.280	<u>0.337</u>	0.290	0.342	0.300	0.345	0.299	0.348	0.280	0.340	0.289	0.343	0.299	0.343
	192	0.318	0.354	<u>0.326</u>	<u>0.365</u>	0.334	0.368	0.335	0.366	0.334	0.373	0.347	0.387	0.332	0.367	0.336	0.367
	336	0.356	0.374	<u>0.362</u>	<u>0.387</u>	<u>0.362</u>	<u>0.384</u>	0.364	<u>0.383</u>	0.370	0.394	0.366	0.405	<u>0.362</u>	0.389	0.367	0.385
	720	0.411	0.412	0.417	0.422	0.425	0.415	0.417	<u>0.413</u>	0.422	0.426	0.403	0.432	<u>0.408</u>	0.420	0.420	0.418
	Avg.	0.342	0.367	<u>0.346</u>	0.378	0.353	<u>0.377</u>	0.354	<u>0.377</u>	0.356	0.385	0.349	0.392	0.348	0.380	0.356	0.378
ETTh2	96	0.161	0.245	0.168	<u>0.252</u>	0.161	0.253	<u>0.162</u>	0.253	0.180	0.263	0.164	0.254	0.165	0.257	0.165	0.260
	192	0.216	0.284	0.223	0.297	0.221	0.296	<u>0.217</u>	<u>0.290</u>	0.236	0.307	0.223	0.295	0.223	0.294	0.219	0.297
	336	0.269	0.318	0.273	0.328	0.272	0.329	<u>0.270</u>	<u>0.325</u>	0.287	0.340	0.279	0.330	0.272	0.333	0.290	0.345
	720	0.354	0.373	0.364	0.386	<u>0.359</u>	0.391	0.361	<u>0.384</u>	0.364	0.391	<u>0.359</u>	0.383	0.363	0.386	0.375	0.403
	Avg.	0.250	0.305	0.257	0.316	<u>0.253</u>	0.317	<u>0.253</u>	<u>0.313</u>	0.267	0.325	0.256	0.315	0.256	0.318	0.262	0.326
ETTh1	96	0.359	0.384	0.375	0.394	0.377	0.397	<u>0.364</u>	<u>0.392</u>	0.380	0.401	0.375	0.398	0.370	0.397	0.368	0.393
	192	0.396	0.411	0.412	0.429	0.413	0.419	<u>0.397</u>	<u>0.413</u>	0.423	0.431	0.407	0.425	0.404	0.423	0.400	0.417
	336	0.413	0.428	0.429	0.443	0.425	0.438	<u>0.422</u>	<u>0.432</u>	0.437	0.450	0.431	0.435	0.423	0.437	0.430	0.441
	720	0.419	0.445	0.447	0.472	<u>0.442</u>	<u>0.456</u>	0.443	<u>0.463</u>	0.460	0.471	0.452	<u>0.456</u>	0.444	0.464	0.477	0.497
	Avg.	0.397	0.417	0.416	0.434	0.414	0.429	<u>0.406</u>	<u>0.425</u>	0.425	0.438	0.416	0.428	0.410	0.430	0.419	0.437
ETTh2	96	0.282	0.329	0.291	0.339	0.281	0.343	0.265	<u>0.334</u>	0.294	0.345	<u>0.280</u>	0.340	0.290	0.342	0.286	0.351
	192	0.342	<u>0.376</u>	0.349	0.390	<u>0.333</u>	0.383	0.324	0.373	0.358	0.395	<u>0.348</u>	0.388	0.354	0.397	0.352	0.394
	336	0.370	0.397	0.381	0.413	0.368	0.411	0.352	<u>0.399</u>	0.385	0.415	<u>0.366</u>	0.405	0.384	0.413	0.439	0.456
	720	<u>0.400</u>	0.428	0.410	0.442	0.407	0.440	0.393	<u>0.432</u>	0.412	0.436	<u>0.404</u>	0.433	0.408	0.442	0.570	0.530
	Avg.	0.348	0.383	0.358	0.396	<u>0.347</u>	0.394	0.334	<u>0.384</u>	0.362	0.398	0.349	0.392	0.359	0.399	0.412	0.433
Weather	96	0.147	0.184	<u>0.143</u>	0.195	0.142	0.195	0.168	0.221	0.155	0.206	0.147	0.197	0.145	<u>0.194</u>	0.170	0.229
	192	0.192	0.228	<u>0.188</u>	<u>0.236</u>	0.186	0.238	0.212	0.258	0.199	0.249	<u>0.190</u>	0.240	0.191	0.237	0.212	0.268
	336	0.240	0.270	<u>0.238</u>	<u>0.276</u>	0.237	0.278	0.258	0.292	0.247	0.284	<u>0.253</u>	0.285	0.243	0.279	0.258	0.307
	720	0.315	0.324	0.312	<u>0.327</u>	<u>0.313</u>	0.330	0.324	0.338	0.318	0.336	0.326	0.339	<u>0.313</u>	0.330	0.321	0.359
	Avg.	<u>0.223</u>	0.251	0.220	<u>0.259</u>	0.220	0.261	0.240	0.277	0.230	0.269	0.229	0.265	<u>0.223</u>	0.260	0.240	0.291
1 st Count		37		3		5		<u>6</u>		0		2		0		0	

Table 22: Results under the hyperparameter search setting described in Appendix Section I. The lookback window is selected from {96, 192, 320, 512}, and the best configuration is reported for each model. This setup ensures that the comparison reflects each model’s optimal performance rather than a fixed setting constraint. As far as we know, we are the first open source parameter search script.

Methods		TimeMosaic	LLMTime	GPT4TS	DLinear	PatchTST				
Metric		MSE MAE	MSE MAE	MSE MAE	MSE MAE	MSE MAE	MSE MAE	MSE MAE	MSE MAE	MSE MAE
<i>ETTh1</i> → <i>ETTh2</i>	96	0.301 0.341	0.510 0.576	0.335 0.374	0.347 0.400	<u>0.304</u> <u>0.350</u>				
	192	0.375 0.387	0.523 0.586	0.412 0.417	0.447 0.460	<u>0.386</u> <u>0.400</u>				
	336	0.411 0.416	0.640 0.637	0.441 0.444	0.515 0.505	<u>0.414</u> <u>0.428</u>				
	720	0.414 0.419	2.296 1.034	0.438 0.452	0.665 0.589	<u>0.419</u> <u>0.443</u>				
	Avg	0.375 0.391	0.992 0.708	0.406 0.422	0.493 0.488	<u>0.380</u> <u>0.405</u>				
<i>ETTh1</i> → <i>ETTh2</i>	96	0.212 0.302	0.646 0.563	0.236 0.315	0.255 0.357	<u>0.215</u> <u>0.304</u>				
	192	0.275 0.328	0.934 0.654	0.287 0.342	0.338 0.413	<u>0.275</u> <u>0.339</u>				
	336	0.331 0.361	1.157 0.728	0.341 0.374	0.425 0.465	<u>0.334</u> <u>0.373</u>				
	720	0.428 0.342	4.730 1.531	0.435 <u>0.422</u>	0.640 0.573	<u>0.431</u> <u>0.424</u>				
	Avg	0.312 0.333	1.867 0.869	0.325 0.363	0.415 0.452	<u>0.314</u> <u>0.360</u>				
<i>ETTh2</i> → <i>ETTh1</i>	96	0.471 0.454	1.130 0.777	0.732 0.577	0.689 0.555	<u>0.485</u> <u>0.465</u>				
	192	0.524 0.483	1.242 0.820	0.758 0.559	0.707 0.568	<u>0.565</u> <u>0.509</u>				
	336	0.586 0.509	1.328 0.864	0.759 0.578	0.710 0.577	<u>0.581</u> <u>0.515</u>				
	720	0.595 0.544	4.145 1.461	0.781 0.597	0.704 0.596	<u>0.628</u> <u>0.561</u>				
	Avg	0.544 0.498	1.961 0.981	0.757 0.578	0.703 0.574	<u>0.565</u> <u>0.513</u>				
<i>ETTh2</i> → <i>ETTh2</i>	96	0.226 0.308	0.646 0.563	0.253 0.329	0.240 0.336	<u>0.226</u> <u>0.309</u>				
	192	0.285 0.341	0.934 0.654	0.293 0.346	0.295 0.369	<u>0.289</u> <u>0.345</u>				
	336	0.340 0.370	1.157 0.728	0.347 0.376	<u>0.345</u> 0.397	<u>0.348</u> <u>0.379</u>				
	720	0.431 0.417	4.730 1.531	0.446 0.429	<u>0.432</u> 0.442	<u>0.439</u> <u>0.427</u>				
	Avg	0.321 0.359	1.867 0.869	0.335 0.370	0.328 0.386	<u>0.325</u> <u>0.365</u>				
<i>ETTh1</i> → <i>ETTh1</i>	96	0.331 0.379	0.510 0.576	<u>0.353</u> 0.392	0.365 0.415	<u>0.354</u> <u>0.385</u>				
	192	0.399 0.420	0.523 0.586	<u>0.443</u> 0.437	0.454 0.462	<u>0.447</u> <u>0.434</u>				
	336	0.418 0.443	0.640 0.637	<u>0.469</u> <u>0.461</u>	0.496 0.494	<u>0.481</u> <u>0.463</u>				
	720	0.416 0.446	2.296 1.034	<u>0.466</u> <u>0.468</u>	0.541 0.529	<u>0.474</u> <u>0.471</u>				
	Avg	0.391 0.422	0.992 0.708	<u>0.433</u> 0.439	0.464 0.475	<u>0.439</u> <u>0.438</u>				
<i>ETTh1</i> → <i>ETTh2</i>	96	0.179 0.267	0.646 0.563	0.217 0.294	0.221 0.314	<u>0.195</u> <u>0.271</u>				
	192	0.237 0.328	0.934 0.654	0.277 0.327	0.286 0.359	<u>0.258</u> <u>0.311</u>				
	336	0.300 0.348	1.157 0.728	0.331 0.360	0.357 0.406	<u>0.317</u> <u>0.348</u>				
	720	0.385 0.377	4.730 1.531	0.429 0.413	0.476 0.476	<u>0.416</u> <u>0.404</u>				
	Avg	0.278 0.330	1.867 0.869	0.313 0.348	0.335 0.389	<u>0.296</u> <u>0.334</u>				

Table 23: Full zero-shot learning results on ETT datasets. A lower value indicates better performance.

Methods	TimeMosaic		TimeMoE _l		TimeMoE _b		MOIRAI _l		MOIRAI _b		Chronos _b		Chronos _s		TimesFM		Moment		
Metric	MSE	MAE	MSE	MAE	MSE	MAE	MSE	MAE	MSE	MAE	MSE	MAE	MSE	MAE	MSE	MAE	MSE	MAE	
ETT _{h1}	96	0.367	0.395	0.350	0.382	<u>0.357</u>	<u>0.381</u>	0.381	0.388	0.376	0.392	0.384	0.379	0.394	<u>0.381</u>	0.414	0.404	0.688	0.557
	192	0.395	0.412	<u>0.388</u>	<u>0.412</u>	0.384	0.404	0.434	0.415	0.412	0.413	0.441	<u>0.412</u>	0.455	<u>0.414</u>	0.465	0.434	0.688	0.560
	336	0.410	0.423	<u>0.411</u>	0.430	<u>0.411</u>	0.434	0.495	0.445	0.433	<u>0.428</u>	0.475	<u>0.430</u>	0.499	0.444	0.503	0.456	0.675	0.563
	720	0.422	0.443	<u>0.427</u>	0.455	0.449	0.477	0.611	0.510	0.447	<u>0.444</u>	0.472	<u>0.446</u>	0.520	0.476	0.511	0.481	0.683	0.585
	Avg	<u>0.399</u>	<u>0.418</u>	0.394	0.419	0.400	0.424	0.480	0.439	0.417	0.419	0.443	0.416	0.467	0.428	0.473	0.443	0.683	0.566
ETT _{h2}	96	<u>0.286</u>	0.346	0.302	0.354	0.305	0.359	0.296	0.330	0.294	0.325	0.289	0.330	0.282	<u>0.328</u>	0.315	0.349	0.342	0.396
	192	0.353	0.389	0.364	0.385	0.351	0.386	0.361	<u>0.371</u>	0.365	0.375	0.359	0.369	<u>0.354</u>	<u>0.373</u>	0.388	0.395	<u>0.354</u>	0.402
	336	<u>0.376</u>	0.411	0.417	0.425	0.391	0.418	0.390	0.390	<u>0.376</u>	0.390	0.399	0.400	0.416	0.410	0.422	0.427	0.356	0.407
	720	<u>0.402</u>	0.435	0.537	0.496	0.419	0.454	0.423	0.418	0.416	0.433	0.420	<u>0.425</u>	0.428	0.431	0.443	0.454	0.395	0.434
	Avg	0.354	0.395	0.405	0.415	0.366	0.404	0.367	0.377	0.362	0.382	0.366	<u>0.381</u>	0.370	0.385	0.392	0.406	<u>0.361</u>	0.409
ETT _{m1}	96	0.392	0.399	0.309	0.357	0.338	0.368	0.380	<u>0.361</u>	0.363	0.356	0.331	<u>0.333</u>	<u>0.328</u>	0.332	0.361	0.370	0.654	0.527
	192	0.422	0.416	0.346	<u>0.381</u>	<u>0.353</u>	0.388	0.412	<u>0.383</u>	0.388	0.375	0.386	0.365	0.365	0.384	0.414	0.405	0.662	0.532
	336	0.450	0.432	0.373	0.408	<u>0.381</u>	0.413	0.436	<u>0.400</u>	0.416	0.392	0.408	0.382	0.391	0.425	0.445	0.429	0.672	0.537
	720	0.500	0.459	0.475	0.477	0.504	0.493	0.462	0.420	<u>0.460</u>	0.418	0.503	<u>0.430</u>	0.445	0.525	0.512	0.471	0.692	0.551
	Avg	0.441	0.427	0.375	<u>0.405</u>	0.394	0.415	0.422	0.391	0.406	0.385	0.407	0.377	<u>0.382</u>	0.416	0.433	0.418	0.670	0.536
ETT _{m2}	96	0.190	0.276	0.197	0.286	0.201	0.291	0.211	0.274	0.205	0.273	0.177	0.244	<u>0.180</u>	0.251	0.202	0.270	0.260	0.335
	192	0.249	0.313	0.250	0.322	0.258	0.334	0.281	<u>0.318</u>	0.275	<u>0.316</u>	<u>0.251</u>	0.293	<u>0.251</u>	0.298	0.289	0.321	0.289	0.350
	336	0.305	0.347	0.337	0.375	0.324	0.373	0.341	0.355	0.329	0.350	0.305	0.327	<u>0.315</u>	<u>0.338</u>	0.360	0.366	0.324	0.369
	720	<u>0.396</u>	0.407	0.480	0.461	0.488	0.464	0.428	<u>0.428</u>	0.437	<u>0.411</u>	0.419	0.394	0.421	0.403	0.462	0.430	0.394	0.409
	Avg	0.285	0.336	0.316	0.361	0.317	0.365	<u>0.315</u>	0.343	0.311	<u>0.337</u>	<u>0.288</u>	0.314	0.291	0.330	0.328	0.346	0.316	0.365
Weather	96	0.178	0.236	0.159	0.213	<u>0.160</u>	0.214	0.278	0.376	0.220	0.217	0.177	<u>0.210</u>	0.172	0.206	-	-	0.243	0.255
	192	0.227	0.279	0.215	0.266	0.210	0.260	0.301	0.409	0.271	0.259	0.224	<u>0.253</u>	0.218	<u>0.248</u>	-	-	0.278	0.329
	336	0.279	0.316	0.291	0.322	0.309	<u>0.309</u>	0.329	0.420	0.286	0.297	0.260	0.276	<u>0.266</u>	0.282	-	-	0.306	0.346
	720	0.351	0.365	0.415	0.400	0.418	0.405	0.370	0.463	0.373	0.354	0.345	0.331	<u>0.358</u>	0.339	-	-	<u>0.350</u>	<u>0.374</u>
	Avg	0.259	0.299	0.270	0.300	0.274	0.297	0.319	0.417	0.287	0.281	0.251	0.267	<u>0.253</u>	<u>0.268</u>	-	-	0.294	0.326
Global Temp	96	0.237	0.366	0.219	0.341	0.230	0.350	0.278	0.376	0.273	0.377	<u>0.236</u>	0.352	0.233	<u>0.348</u>	0.255	0.375	0.363	0.472
	192	0.288	0.409	0.265	0.381	0.268	0.385	0.301	0.409	0.304	0.409	<u>0.287</u>	0.398	<u>0.287</u>	<u>0.397</u>	0.313	0.423	0.387	0.489
	336	0.341	0.449	0.326	0.426	0.326	<u>0.427</u>	0.329	<u>0.420</u>	0.332	0.437	0.332	0.433	<u>0.320</u>	0.430	0.362	0.460	0.430	0.517
	720	0.479	0.542	0.344	0.453	0.377	0.467	0.379	0.467	0.379	0.469	<u>0.463</u>	0.524	0.452	<u>0.521</u>	0.486	0.545	0.582	0.617
	Avg	0.336	0.442	0.288	0.400	<u>0.300</u>	0.407	0.321	<u>0.418</u>	0.322	0.423	0.329	0.426	0.323	0.424	0.354	0.451	0.440	0.524

Table 24: Zero-shot forecasting results on six datasets. TimeMosaic is trained with an input length of 512 and an output horizon of 720. The symbols *s*, *b*, and *l* represent the small, base, and large versions, respectively.

Dataset		z-score		RevIN	
		MSE	MAE	MSE	MAE
ETTh1	96	0.304	0.344	0.299	0.340
	192	0.339	0.364	0.341	0.365
	336	0.375	0.385	0.359	0.380
	720	0.422	0.413	0.424	0.414
ETTh2	96	0.165	0.249	0.164	0.247
	192	0.230	0.290	0.226	0.291
	336	0.282	0.327	0.279	0.324
	720	0.356	0.374	0.353	0.376
ETTh1	96	0.362	0.387	0.358	0.386
	192	0.400	0.411	0.398	0.410
	336	0.436	0.435	0.435	0.435
	720	0.451	0.460	0.481	0.480
ETTh2	96	0.300	0.342	0.302	0.342
	192	0.354	0.387	0.356	0.386
	336	0.378	0.403	0.378	0.402
	720	0.421	0.439	0.438	0.451
Weather	96	0.144	0.241	0.152	0.189
	192	0.197	0.232	0.192	0.229
	336	0.245	0.276	0.245	0.272
	720	0.327	0.327	0.328	0.328
Electricity	96	0.140	0.236	0.140	0.236
	192	0.156	0.250	0.155	0.250
	336	0.173	0.267	0.173	0.267
	720	0.212	0.298	0.212	0.298
Traffic	96	0.410	0.276	0.409	0.274
	192	0.424	0.281	0.424	0.280
	336	0.435	0.287	0.437	0.287
	720	0.464	0.302	0.464	0.301
Solar-Energy	96	0.200	0.226	0.204	0.222
	192	0.225	0.244	0.223	0.235
	336	0.238	0.245	0.236	0.238
	720	0.241	0.251	0.236	0.243

Table 25: Forecasting performance (MSE and MAE) under z-score vs. RevIN normalization across eight datasets.

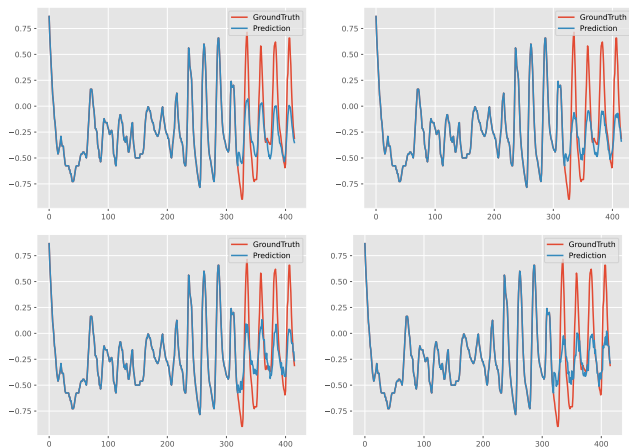


Figure 15: Prediction cases from ETTh2 by different models (TimeMosaic, SimpleTM, PatchTST, iTransformer) under input-320-predict-96 settings.

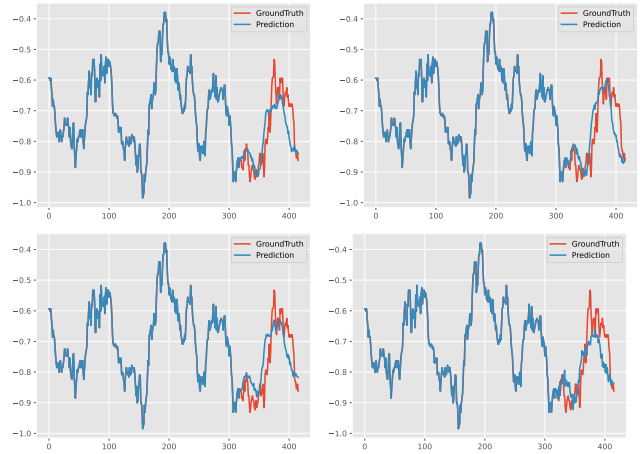


Figure 16: Prediction cases from ETTh1 by different models (TimeMosaic, SimpleTM, PatchTST, iTransformer) under input-320-predict-96 settings.

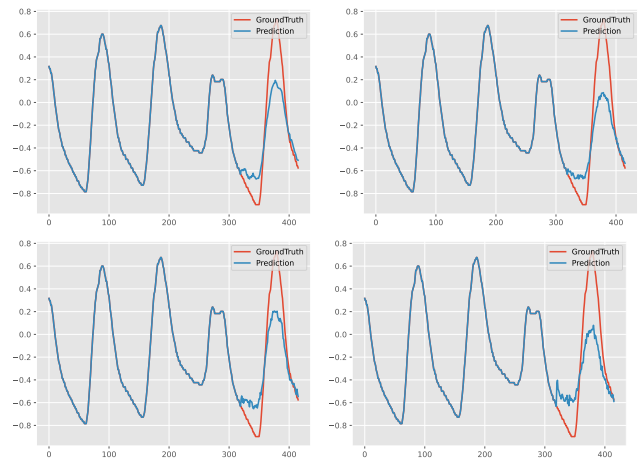


Figure 17: Prediction cases from ETTm2 by different models (TimeMosaic, SimpleTM, PatchTST, iTransformer) under input-320-predict-96 settings.